The Henkel Petrophysical Plot: Mineralogy and Lithology from Physical Properties

Randolph Jonathan Enkin[1], Tark Scott Hamilton[1], and William Morris[2]

[1]Geological Survey of Canada
[2]McMaster University

November 24, 2022

Abstract

The Henkel plot (logarithm of magnetic susceptibility versus density of rock samples) reveals that most rocks fall on either a "magnetite trend" or a "paramagnetic trend". Interpretation of gravity and magnetic surveys is improved when the mineralogical and lithological basis of these trends is understood. We present a quantitative mineralogical mixing model, involving the components QFC (quartz-feldspar-calcite), FM (ferromagnesian silicates), and M (magnetite), and discuss the geological processes which produce or modify these mixtures. Igneous rocks mostly plot on the magnetite trend, where the FM/M ratio is about 10. The density-susceptibility mineralogical mixing model is compatible with the CIPW mineral calculation for igneous classification from chemical analyses. Sedimentary and metamorphic processes usually involve oxidation, reduction, and/or iron loss, all which are magnetite-destructive and lead to petrophysical measurements along the paramagnetic trend where FM/M >1000. Mineralization, with the introduction of sulfides and oxides leads to dense rocks which do not plot along the magnetite nor paramagnetic trends. This quantitative analysis provides a method to integrate geological processes in the interpretation of geophysical surveys.

The Henkel Petrophysical Plot: Mineralogy and Lithology from Physical Properties

Randolph J. Enkin[1], Tark S. Hamilton[2], and William A, Morris[2]

[1]Geological Survey of Canada – Pacific, Sidney, BC V8L 4B2, Canada

[2]School of Geography and Earth Sciences, McMaster University, Hamilton, ON L8S 4L8, Canada

Corresponding author: Randolph J. Enkin (randy.enkin@canada.ca)

Key Points:

- The Henkel plot (logarithm of magnetic susceptibility versus density of rock samples) helps integrate geological and geophysical analysis.
- We present a quantitative mineralogical mixing model involving 3 components Quartz-Feldspar-Calcite, Ferromagnesian silicates and Magnetite.
- Major geological processes leading to petrophysical properties on different regions of the Henkel plot are easily explained.

Abstract

The Henkel plot (logarithm of magnetic susceptibility versus density of rock samples) reveals that most rocks fall on either a “magnetite trend” or a “paramagnetic trend”. Interpretation of gravity and magnetic surveys is improved when the mineralogical and lithological basis of these trends is understood. We present a quantitative mineralogical mixing model, involving the components QFC (quartz-feldspar-calcite), FM (ferromagnesian silicates), and M (magnetite), and discuss the geological processes which produce or modify these mixtures. Igneous rocks mostly plot on the magnetite trend, where the FM/M ratio is about 10. The density-susceptibility mineralogical mixing model is compatible with the CIPW mineral calculation for igneous classification from chemical analyses. Sedimentary and metamorphic processes usually involve oxidation, reduction, and/or iron loss, all which are magnetite-destructive and lead to petrophysical measurements along the paramagnetic trend where FM/M >1000. Mineralization, with the introduction of sulfides and oxides leads to dense rocks which do not plot along the magnetite nor paramagnetic trends. This quantitative analysis provides a method to integrate geological processes in the interpretation of geophysical surveys.

Plain Language Summary

The Henkel plot (logarithm of magnetic susceptibility versus density of rock samples) is useful for linking geophysical data and geological interpretation. Our study merges thousands of rock physical properties measurements with their corresponding rock types and minerals. Given this globally applicable database, we calibrated a model reducing these many parameters to 3 basic groups of minerals and their physical properties. This model permits users of remote sensing data to come up with equivalent rock and mineral types and a spatial view of geological processes. It also allows geochemical data on igneous rocks to predict their physical behaviour and control on regional geophysical mapping.

1 Introduction

Effective geophysical mineral exploration, after decades of simply “drilling targets”, now requires an integrated approach to understanding the geochemistry, mineralogy, lithology, and geological processes that form the deposit system (McCuaig and Hronsky, 2014). In this paper, we move beyond simple categorization of rock types according to their physical properties, to developing mineral models and interpreting geological processes in terms of physical properties that can be measured in the laboratory and determined from geophysical surveys.

Dentith et al. (2017, 2019) provide a conceptual framework for petrophysical data by placing the various rock physical properties on a ternary diagram (Fig. 1) with end members of “Bulk (overall composition), “Grain (amount, size, shape of minority mineral phases)”, and “Texture (geometric relationships between grains)”. Density is dominated by the Bulk composition, whereas magnetic susceptibility is dominated by the concentration of the minor mineral magnetite, a Grain parameter. In Dentith’s (op cit.) framework, Texture includes porosity and permeability which dominate electrical conductivity. Different physical properties are controlled by complementary aspects of rocks, and individual rock types are better characterized when more than one physical property is recorded.

Rock physical properties provide the link between geophysics and geology. Physical properties are rapid to measure, reproducible, and afford numerical values that can be spatially referenced and analysed. They are the key to providing physical ground truth and characterization of diverse rock types. Mahmoodi and Smith (2015) for example, apply fuzzy k-means clustering on borehole susceptibility, density and gamma logs to characterise lithological zones in the Sudbury Intrusive Complex. These data, especially density and magnetic susceptibility when correlated to lithologies and mineralogies are essential inputs to constrain the geophysical inversion and geological interpretation of magnetic and gravity surveys (Vallée et al., 2019a and b). In this paper we dissect systematic changes in density and magnetic susceptibility, and how these relate to geological processes including igneous rock formation, weathering and sedimentary transport, metamorphism, alteration, and ore formation. We show that it is possible to explain most changes in density and magnetic susceptibility by considering the volume concentrations of three principal groups of minerals, QFC (quartz-feldspar-calcite), FM (ferromagnesian silicates), and M (magnetite). We offer an example of a porphyry copper deposit which demonstrates the geophysical responses due to the lithological sequence in a differentiating intrusion and to its subsequent metamorphism and mineralization.

2 Background

Gravity surveys reveal variations caused by contrasts in rock density. Geologically abundant rock types such as granodiorite, gabbro, sandstone and greenschist (Wyllie, 1971) are composed of relatively few minerals with common minerals having a limited range of densities (Fig.2). Most rock densities, particularly in continental shield areas and eroded orogenic belts, range from 2.6 to 2.8 g/cm^3. Hinze (2003) recommended that a density value of 2.67 g/cm^3 should be used for Bouguer anomaly correction. More recently, Tschirhart et al., (2019) demonstrated that optimal Bouguer correction (minimization of terrain-related signal) is best achieved with a spatially varying density value. Even so the densities they used only varied from 2.72 to 2.83 g/cm^3. While ore minerals can be appreciably denser (4 to 19 g/cm^3), they rarely comprise more than a few percent of regionally extensive rock (Fig.2). When present as a significant concentration, as in a mineral deposit, the sulfides can lead to an enhanced gravity signature (Thomas, 2003).

Magnetic surveys provide high-resolution aerial coverage that often contain diagnostic spatial patterns capable of distinguishing lithologies, faults, intrusions and blocks of crust with distinctive tectonic or thermal histories (Gunn and Dentith, 1997, Airo, 2015). This survey tool is particularly powerful when coupled with well-understood physics and well-developed mathematical techniques (filtering, upwards or downwards continuation, Euler deconvolution, etc.) that permit estimates of depth to basement or Curie isotherms, location and geometry of plutons, dykes, fracture systems and ore bodies (Grant 1984a, 1984b). For regions where the Koenigsberger ratio is low (that is, induction is greater than remanence for magnetic sources), the interpretation depends on contrasts in magnetic susceptibility (Morris et al., 2007). While there are a variety of magnetic minerals, the strongest, most abundant, and most widespread is magnetite. Locally relevant interpretation requires physical measurements of magnetic susceptibility of the significant lithologies and their variation. Clark (1997) provides a comprehensive outline of magneto-petrophysics describing the various types of magnetism (dia-, para- and ferro-magnetism), how they relate to magnetic mineralogy, and how magnetic properties of rocks vary as a function of primary (magmatic) and secondary (sedimentary, metamorphic) processes. Different episodes of ferromagnetic minerals (Balsley and Buddington,

1958) or other geological and mineralogical processes leading to the formation of ore deposits (e.g., porphyry copper, ultramafics, and skarns) can generate diagnostic patterns of rocks with enhanced or diminished magnetite content apparent as different geometries on magnetic maps Clark et al., 1992).

Oxygen is by far the most common element in earth materials and, given its large atomic radius as oxides or other oxyanions (silicate, carbonate, sulfate), it provides the volume framework for most minerals. It comprises about 46.6% of the Earth's crust by weight and more than 90% of the crust by volume (Barth, 1948). Oxygen ions form hexagonal and cubic packing structures which readily accommodate smaller mineral-forming cations: Si^{4+}, Al^{3+}, Fe^{2+}, Fe^{3+}, Mg^{2+}, Ca^{2+} etc., in either the smaller tetrahedral sites (surrounded by 4 oxygens) or the larger octahedral sites (surrounded by 6 oxygens). Oxide and silicate minerals often crystallize in epitaxis, wherein two adjacent minerals share a single planar face with a plane of oxide anions as their common boundary. It is thus common for many minerals to crystallize with inclusions of different minerals. This is particularly important for magnetite since sub-microscopic inclusions of magnetite can impart measurable ferromagnetic properties to otherwise paramagnetic or diamagnetic enclosing host-mineral phases (Haggerty, 1979; Fleet et al., 1980; Feinberg et al., 2005).

Iron is both the most common heavy element and the most common magnetic element in the Earth's crust. Thus, much of the discussion of density and magnetic susceptibility reduces to an analysis of the disposition of iron and its oxidation states. Ferromagnesian silicates (including olivine, pyroxene, amphibole, biotite) have up to about 40% Fe by weight, but usually have more Mg than Fe. Most of the crust sits at or slightly above (i.e., more oxidized than) the Fayalite-Magnetite-Quartz (FMQ) oxygen buffer (Eugster, 1957; Robie et al., 1982). This buffer controls the fugacity (chemical activity) of O_2 via the following mineral assemblage:

$$3\ \text{Fayalite}\ (Fe^{2+}{}_2SiO_4) + O_2 = 3\ \text{Quartz}\ (SiO_2) + 2\ \text{Magnetite}\ (Fe^{2+}Fe^{3+}{}_2O_4). \qquad \text{[eq.1]}$$

Here, fayalite represents the class of ferrous (Fe^{2+}) FM silicate minerals. At higher oxygen fugacity, all the ferric iron (Fe^{3+}) and a fraction of the ferrous Fe^{2+} combine to form magnetite (Fe_3O_4). Oxygen as 21% of the atmosphere and ~10 ppm dissolved in shallow oxygenated surface waters is the most common oxidant. As a result, uplift and exposure of magnetite-bearing rocks often oxidizes magnetite to maghemite, hematite or less-magnetic ferric oxy-hydroxides. Rocks formed in reducing and sulfidizing environments lose magnetite and tend to form iron sulfides such as non-magnetic pyrite, and locally strongly magnetic pyrrhotite, and other iron bearing ore minerals (Worm et al., 1993, Clark and Tonkin, 1994).

3 The Henkel Plot

The cross-plot of the logarithm of magnetic susceptibility against density for rock samples, reveals contributions from the constituent minerals, and the imprint imposed by a variety of geological settings and processes through the measurements of two common and easily measured petrophysical properties. Henkel (1976) published the first known such plot. Enkin (2018) compiled 59 of these plots published in 26 publications using data from five continents, and presents a further 20 based on various aspects of the Canadian Rock Physical Property Database (CRPPD). The remarkable property all these plots have in common is that most of the measurements fall on two relatively well-constrained bands (Fig. 3), which Henkel (1991) recognized and named the "paramagnetic trend" and the "magnetite trend". Because of

Herbert Henkel's leadership in the use and analysis of this plot, Dentith et al., (2017) named it the "Henkel plot".

The current CRPPD is not a comprehensive nor a homogeneous compilation of Canadian geology. The data set is biased by the research goals of the geologists, mostly involved with mineral exploration, who have collected and submitted samples and measurements. Furthermore, since the compilation started as a database for the province of British Columbia (Enkin, 2014), it has a geographic bias in a region containing rocks of relatively low metamorphic grade. Nevertheless, the features present in the CRPPD Henkel plot are apparent in the global compilation of Henkel plots (appendix of Enkin, 2018), and correspond to common rock and mineral forming processes, so we contend that the detailed analysis and interpretations of the CRPPD Henkel plot are valid for most geological settings.

Grain density refers to the density of the minerals in a rock, while saturated bulk density includes the effect of rock porosity filled with water (with the limitation that laboratory measurements fail to fill blind porosity with water). The Henkel plot of the CRPPD presents 3770 points of magnetic susceptibility against grain density (Fig. 3a) and 11146 measurements using saturated bulk density (Fig. 3b). With the high concentration of points plotting on top of one another, it is best to analyse these features using iso-concentration contours, such as included on Figure 3. The Henkel plot displays two modes sitting along two curved trends. Using the grain density version, the modes are at (2.67 g/cm^3, $1.9 \cdot 10^{-2}$ SI), and (2.74 g/cm^3, $2.6 \cdot 10^{-4}$ SI). The corresponding modes on the saturated bulk density version are similar: (2.66 g/cm^3, $1.9 \cdot 10^{-2}$ SI), and (2.73 g/cm^3, $2.7 \cdot 10^{-4}$ SI). The "magnetite trend" denotes the curved band that passes through the higher susceptibility mode, while the band passing through the lower susceptibility mode is the "paramagnetic trend" (Henkel, 1991).

Enkin (2018) displayed Henkel plots for many different rock types and suites of related rocks to demonstrate features of their distribution. In summary, most igneous rocks plot near the upper mode and along the magnetite trend. Plutonic rocks follow the magnetite trend quite closely, while a significant proportion of volcanic rocks plot off the trend due to lower densities because of vesicles or other pore space. Felsic rocks have lower iron content and thus tend to have lower density and magnetic susceptibility than mafic rocks. Most sedimentary and metamorphic rocks plot along the paramagnetic trend, but both classes feature a subpopulation plotting along the magnetite trend due to immature lithic clasts and placers. For example, Parker Gay and Hawley (1991) report aeromagnetic anomaly patterns associated with sediments from three areas: in each of these examples the sediments are magnetite rich as a result of nearby volcanic activity. Sediments often plot at lower densities than metamorphic rocks because of their porosity and low iron content, while the metamorphic rocks have a tighter distribution along the paramagnetic trend. Intensely mineralized and altered rocks have much more scattered distributions with respect to the two main trends.

4 Mineral Modelling

4.1 Forward Modelling

In geochemical analyses, it is often useful to plot "mineral mixing lines" on bivariate plots or ternary diagrams to indicate the proportions of end-member minerals. This modelling approach is particularly useful wherein the variation in rock types is due to mixing or fractionation, as in the tholeiitic or calc-alkaline trends on either the AFM (Alkali, Iron,

Magnesium) diagram or the Total Alkalis versus Silica (TAS) plot (Irvine and Baragar, 1971; Le Maitre et al., 2005). Streckeisen (1976) constructed a classification scheme for igneous rocks based on the presence of five mineral groups: quartz (Q), alkali feldspar (A), plagioclase (P), feldspathoids (F), and mafic minerals (M). We use a similar end-member mineral modelling approach to calibrate the natural span of rock density and susceptibility variations and their mineral properties on the Henkel plot. We remark that there is a restricted natural span of densities for common rock forming minerals between non-ferromagnesian silicates and ferromagnesian silicates comprising the range of most rocks (Fig. 2). Additionally, the magnetite content, ranging between several percent down to trace amounts, dominates their magnetic susceptibility. Note, throughout this paper, mineral proportions are given in volume percent, which is better linked to density and magnetic susceptibility of bulk rocks than is weight percent.

Trends on the Henkel plot can be quantitatively analysed in terms of mixing models for the groups of minerals which control their physical properties (Henkel, 1991; Williams and Dipple, 2007; Williams, 2009). The interpretive value of a mineralogically calibrated Henkel plot is that magnetic and gravity potential field data can yield lithologies and geological processes based on the mineralogical calibrations. Looking at density and susceptibility data with a mineralogically calibrated Henkel plot permits discrimination between mafic and felsic volcanics, localized zones of metamorphism, zones of increased fracture density. For the purpose of this analysis, we propose that most common non-porous and non-mineralized rocks are described as combinations of three end-member groups of minerals (QFC-Quartz-Feldspar-Calcite, FM-Ferromagnesian silicates, M-Magnetite). While it may not be obvious that such mineral groups can, or should, be modelled as single points on the Henkel plot, we demonstrate that this approach is useful for geological-geophysical interpretation, thus justifying the analysis. The remainder of the dispersion in densities on the Henkel plot require two additional qualifications: rocks with significant porosity contain voids or fluids will reduce the bulk density, and rocks containing atypically high concentrations of metals such as sulfides or other ore minerals will exhibit greater densities.

Our approach is similar to Principal Component Analysis, where co-varying variables are gathered together to reduce the number of parameters to describe a system. The three end-member mineral groups we propose have distinct physical and geological properties. In the forward sense, if one knows the proportions of these mineral groups comprising a rock, then the physical properties of that rock can be predicted. In the inverse sense, if one knows the two physical properties of density and magnetic susceptibility, then the range of compatible lithologies can be inferred. As in all earth sciences, there are different advantages to splitting and lumping sets of observations. The goal in our analysis here is to provide an optimal set of usable parameters for linking geophysical and geological analyses for the two dominant trends and the majority of rock types. Forcing the calibration to accommodate all possible outliers needlessly complicates the analysis without providing better insight.

Most crustal rocks have low densities around 2.6-2.8 g/cm^3 due to containing at least half and often more than 90% quartz (2.62 g/cm^3), plagioclase feldspar to alkali-feldspar (2.56-2.76 g/cm^3), and calcite (2.71 g/cm^3) (Fig. 2). These minerals are collectively abbreviated as the "QFC" component. We use the low susceptibility tail of sedimentary rocks in the grain density Henkel plot of the CRPPD (Fig. 3a) as the QFC density endpoint at 2.64 g/cm^3. In addition to being low density, these minerals are characteristically diamagnetic (negative magnetic susceptibility, around -10^{-5} SI). For the pragmatic reason of needing the points to plot on a

logarithmic magnetic susceptibility scale on the Henkel plot, and thus positive, we model the QFC end member with a positive but negligible value of $1.0 \cdot 10^{-7}$ SI.

Igneous rocks are classified mainly by their total proportion of Ferromagnesian silicates (FM). The modal and normative classification of igneous rocks assigns rock names according to normative colour index (CI=proportion of dark coloured FM silicate minerals: mostly olivine, pyroxene, amphibole, biotite) (Bowen, 1922, Irvine and Baragar, 1971, Streckeisen, 1976). This method is readily applied using either visual or chemical estimates. FM minerals display a wide range of densities and susceptibilities (Fig. 2, 4), but most of the rock property distribution on the Henkel plot are well-characterized when we use the point (3.33 g/cm^3, $1.0 \cdot 10^{-3}$ SI) as the FM endpoint, around the density of olivine (92.5% forsterite + 7.5% fayalite). This density also corresponds to peridotite xenoliths from continental cratons (Kelly, et al., 2003) and for our xenolith collection from the Canadian cordillera. We have examined the mineralogy of a variety of rocks in our collection, which plot near the high-density end of the paramagnetic trend, with density around 3.0 g/cm^3 and we see that they typically contain around 20% of QFC minerals, requiring the density of the FM endpoint to be around 3.33 g/cm^3.

It is common for mafic plutonic rocks with high iron content (up to several percent) and abundant ferromagnesian minerals such as pyroxenes to contain sub-microscopic (<100 nm) inclusions of magnetite (Haggerty, 1979; Fleet 1980; Puga et al., 1999; Harrison et al 2002; Feinberg et al 2004, 2005). This inherent characteristic contributes to the low but measurable magnetic susceptibility along the paramagnetic trend. The magnetic susceptibility of individual minerals (e.g., Bleil and Petersen, 1982; Carmichael, 1989; Biedermann, 2018) displays more variability than does their density, but the susceptibility axis of the Henkel plot spans more than 6 orders of magnitude, so the FM endpoint susceptibility value could be higher or lower by a factor of 2 without significantly modifying the analysis or conclusions.

The third end-member is magnetite (M), the most common magnetic mineral and the source of most magnetic susceptibility and remanence in Earth's crust. It has a density of 5.2 g/cm^3 and a remarkably grain size-independent magnetic susceptibility of 3.0 SI (Heider et al., 1996; Peters and Dekkers, 2003). Note that while the intrinsic susceptibility of magnetite is much higher, each grain's individual demagnetizing field diminishes the externally measured susceptibility (Dunlop and Ozdemir, 1997, p. 237). In this context, the shape of the magnetite grains is important. The demagnetizing field along the long axis of acicular grains is lower than that for equant grains, so in rare cases it is possible to measure magnetite susceptibility up to about 6 SI.

The three end-points and mixing curves for the three end members are indicated on Figure 4. The mineral mixing line between the QFC and FM end-points would be a straight line on a linear plot of density vs. magnetic susceptibility, but it takes a curved shape on the density versus log(magnetic susceptibility) Henkel plot. Our QFC-FM mineral-mixing curve traces through the middle of the band labelled "Biotite Amphibole Paramagnetic Trend" in Henkel's (1991) figure 1. In dashed lines, Henkel plotted curves of increasing magnetite starting from no magnetite at the paramagnetic trend, going up as the high susceptibility and density of magnetite substitutes for the paramagnetic component. At the zero-magnetite limit, he marked the "Silicate Density", that is, the density that a rock would have if all the magnetite were removed. Note, there is a simple typographical error on page 4 of Henkel (1991) in the denominator of the equation for silicate density. It should read:

$$d_S = (d - d_M s/s_M)/(1 - s/s_M), \qquad \text{[eq.2]}$$

where d_S is the silicate density, d is the observed or total density, s is the observed susceptibility, d_M is the density of magnetite and s_M is the susceptibility of magnetite. The equation reasonably assumes that the magnetic susceptibilities of the QFC and FM components are negligible.

There are two useful sets of mineral mixing lines illustrating our 3-component mineralogical model on the Henkel plot (Fig. 5a and b). They both display the lines with the range of QFC proportions from 0 to 100% in 10% steps, with the remainder of the rock being the sum of FM and M. In Figure 5a, logarithmic steps of magnetite content, M, are drawn. Above M= 0.03%, these curves are nearly horizontal, with the implication that the magnetic susceptibility is hardly sensitive to any mineralogical components other than the magnetite. That is, rocks containing greater than 0.03% magnetite will have a magnetic susceptibility above 10^{-3} SI, with their density being controlled by the content (percentage) of QFC minerals. Below M=0.03%, the concentration of paramagnetic FM minerals dominate the magnetic susceptibility, with the understanding that FM silicates include submicroscopic magnetite inclusions. Aydin et al., (2007) defined a parameter Maximum Paramagnetic Susceptibility, calculated on basis of density, Fe^{2+}, Fe^{3+}, and Mn^{2+} content, which estimates paramagnetic susceptibility assuming ferromagnesian minerals (biotite and amphibole). In a study of Turkish granitoid rocks the maximum paramagnetic susceptibility identified by Aydin et al., (2007) is $2.4 \cdot 10^{-4}$ SI which is compatible with our model analysis.

Curves of constant FM:M ratio are plotted in Figure 5b. These lines slide from the QFC+M curve (i.e., FM:M=0:1) to the QFC+FM curve (i.e., FM:M = ∞:1). We see that the Magnetite Trend approximates the FM:M = 10:1 mixing model, with the more felsic rocks (that is, high QFC) being more magnetite rich with respect to the FM minerals. The paramagnetic trend is similar to the FM:M = 10000:1 mixing model. There are notably few rocks in the FM:M = 100:1 to 1000:1 range, which is an important feature we will explain.

Figure 6 presents the common projections away from the (QFC, FM, M) mineral model. The curves for the paramagnetic trend (QFC+FM) and the magnetite trend (QFC + a 10:1 ratio of FM:M) are displaced by the given proportion of water (blue curves), pyrite (brown curves) or sphalerite (orange curves). Water-filled porosity accounts for points on the low-density side of the Henkel plot. Most sedimentary rocks in the CRPPD have <10% porosity, while vesicular volcanic rocks can have >30% porosity. Were the CRPPD rock collection more focussed on hydrocarbon reservoir rocks, we would display many more high porosity sedimentary rocks. The mineral-mixing curve for QFC and pure magnetite should limit where rocks plot on the Henkel plot. Rocks that plot at lower density than this mixing line may contain a large proportion of low-density minerals such as K-feldspar (density 2.56 g/cm^3 as in syenites, porphyries, arkoses or K-metasomatized rocks) or graphite, but more likely contain clay minerals, zeolites, or are porous due to fractures and voids and filled with air or water. If magnetite is in an acicular form, then its magnetic susceptibility can be higher by up to a factor of 2, accounting for the few points which lie above the main magnetite trend. The collection of rocks in the CRPPD which contains rocks which notably plot above the QFC-magnetite mixing curve come from the Great Bear Magmatic Zone setting from the Northwest Territories (Enkin et al., 2016). These “Iron Oxide Copper Gold” (IOCG) mineralized rocks include high concentrations of magnetite formed under metasomatic conditions with steep thermal gradients which lead to highly acicular crystal growth.

Rocks that plot with density greater than the mineral mixing curves or susceptibility below them cannot be modelled using the (QFC, FM, M) end-members. These substantially mineralized rocks are rare in the CRPPD (Enkin, 2018, figure 16e). They contain a significant concentration of high-density minerals (>3.7 g/cm^3) with a wide range of magnetic susceptibility (pyrite and sphalerite illustrated in Fig. 6). In a regional context mineralized rocks are rare, however, in some mineral exploration settings it is possible to have significant concentrations of pyrrhotite which influences the observed magnetic anomaly pattern reflecting the enhanced susceptibility of this mineral (Schwarz, 1974 and 1991; Clark, 1984). While mineralized samples are over-represented in the CRPPD, they are still rare enough not to affect the iso-concentration contours on which the mineral-mixing models are based. The mineral explorationist needs to know typical values for ordinary rocks in order to recognize when geophysical inversions produce exotic or unreasonable values.

4.2 Inverse Modelling

Our discussion shows that most rock properties on the Henkel plot is modelled in terms of the three end members. We can invert this model to provide petrophysically estimated mineral concentrations, for rocks that plot within the QFC-FM-M mixing curves as per Figure 4. For simplicity of notation: Q represents the QFC concentration, F represents FM, and M is simply the M magnetite concentration. The three relationships in three unknowns:

$$Q + F + M = 1 \quad , \qquad \text{[eq. 3]}$$

$$d_Q Q + d_F F + d_M M = d, \qquad \text{[eq. 4]}$$

$$s_Q Q + s_F F + s_M M = s, \qquad \text{[eq. 5]}$$

where d stands for density and s stands for magnetic susceptibility, are combined as:

$$\begin{pmatrix} 1 & 1 & 1 \\ d_Q & d_F & d_M \\ s_Q & s_F & s_M \end{pmatrix} \begin{pmatrix} Q \\ F \\ M \end{pmatrix} = \begin{pmatrix} 1 \\ d \\ s \end{pmatrix}. \qquad \text{[eq.6]}$$

Thus

$$\begin{pmatrix} Q \\ F \\ M \end{pmatrix} = \begin{pmatrix} 1 & 1 & 1 \\ d_Q & d_F & d_M \\ s_Q & s_F & s_M \end{pmatrix}^{-1} \begin{pmatrix} 1 \\ d \\ s \end{pmatrix} = \begin{pmatrix} 1 & 1 & 1 \\ 2.64 & 3.33 & 5.2 \\ 10^{-7} & 10^{-3} & 3 \end{pmatrix}^{-1} \begin{pmatrix} 1 \\ d \\ s \end{pmatrix}, \qquad \text{[eq. 7]}$$

which is easily solved with standard software packages, such as numpy.linalg.solve for Python:

$$\begin{pmatrix} Q \\ F \\ M \end{pmatrix} = \begin{pmatrix} 4.8295 & -1.4506 & 0.90450 \\ -3.8308 & 1.4511 & -1.2382 \\ 1.2768 \cdot 10^{-3} & -4.8364 \cdot 10^{-4} & 0.33375 \end{pmatrix} \begin{pmatrix} 1 \\ d \\ s \end{pmatrix}. \qquad \text{[eq. 8]}$$

For example, a granodiorite with density d=2.71 g/cm^3, and magnetic susceptibility s=3.2·10^{-2} SI, is composed of (4.8295*1)+(-1.4506*2.71)+(0.90450*3.2·10^{-2})=92.7% QFC, 6.2% FM, and 1.1% Magnetite. An amphibole schist with density d=3.05 g/cm^3, and magnetic susceptibility s=8.1·10^{-4} SI is composed of 40.6% QFC, 59.4% FM, and just 72ppm Magnetite.

When d and s are outside the mixing model, then the derived Q, F, and M values are outside the 0 to 1 range. The situation happens when: 1) porosity makes the density too low; 2) the rock contains high density, low susceptibility minerals; and/or 3) the model end-members are

not appropriate for the rock's mineralogy. In particular, rhyolites and granites often have high proportions of K-feldspar (density 2.56 g/cm^3) in their QFC composition. When the density of such rocks is below 2.64 g/cm^3, the inverse model equation 8 renders negative concentrations of FM silicates and over 100% QFC. When there are geological reasons to consider the QFC component to be dominated by minerals with density 2.56 g/cm^3, the modified matrix of composition as a function of density and susceptibility becomes:

$$\begin{pmatrix} Q \\ F \\ M \end{pmatrix} = \begin{pmatrix} 4.3274 & -1.2998 & 0.81045 \\ -3.3285 & 1.3002 & -1.1442 \\ 1.1093 \cdot 10^{-3} & -4.3335 \cdot 10^{-4} & 0.33371 \end{pmatrix} \begin{pmatrix} 1 \\ d \\ s \end{pmatrix}. \qquad \text{[eq. 9]}$$

Note, however, that for most of the crust, a QFC density of 2.64 g/cm^3. Using this quartz-dominated value, the QFC-FM mixing curve follows the lower point concentration contour of the paramagnetic trend, and the FM/M=10 mixing curves follows the dominant ridge of the magnetite trend.

The end-member density and magnetic susceptibility values rely on mineral measurements, but particularly for the FM end-member, it is reasonable to question the use of a single point to represent the vast range of rock types and processes. Here we appeal to the "ground truth" of comparison of the petrophysical estimate of the mineralogy to that visually observed in rocks in our collection or derived using normative mineralogy algorithms from the geochemistry. We find that the petrophysically-derived mineralogy is remarkably accurate for the purpose of the geophysical interpretations that we wish to produce.

5 Geological Interpretation

The most abundant crustal elements, in order, are O, Si, Al, Fe, and Ca, with lesser Mg, Na, K and P. All other constituents are minor or trace elements. Iron, with an average crustal value of 5.63% and common range of 1 to 15% by volume (Taylor, 1964), is the most common heavy element and only common magnetic element. As such, the distribution and oxidation state of iron in the mineralogy of rocks plays a dominant role both for a rock's density and its magnetic susceptibility.

The Quartz-Feldspar-Calcite (QFC) family of minerals can hold at most trace amounts of iron in their crystal structures. Nearly all the total iron in rocks is distributed between the Ferro-Magnesian Silicate (FM) family, Magnetite (M), and other oxides and sulfides. Since Fe is the predominant chemical component in rocks with more than one possible valence state, the proportions of ferrous and ferric iron in the bulk chemical analysis of minerals and rocks define oxygen fugacity. Over widespread geological conditions where FM silicate minerals form, the silicates require octahedrally coordinated ferrous iron (Fe^{2+}) for their structures (Deer et al, 1997; Siever and Woodford, 1979). The smaller ferric iron (Fe^{3+}) component goes into magnetite and ensures that magnetite is a primary mineral comprising 0.1 to 3% of most igneous rocks. Natural mineral buffering assemblages, particularly FMQ have been extensively studied and applied to diverse igneous rocks (Carmichael and Nicholls, 1967, Frost and Lindsley, 1991, Frost et al, 1988). Other than oxidizing conditions of surface weathering environments, most iron-bearing minerals are predominantly ferrous (Deer et al., 2011). The ferric iron ions mostly form magnetite and hematite, or other surface weathering oxy-hydroxides like goethite or limonite, in proportions determined by the oxidation state.

Thus for most rocks, there is a high ratio of Fe^{2+}/Fe^{3+}, as verified by abundant empirical data (Marakushev, 1975, Middlemost, 1986) and consistent with the FMQ oxygen fugacity buffer (Eugster, 1957; Fudali, 1965). While total Fe can be readily analysed spectroscopically by techniques including atomic absorption, X-ray fluorescence, and ICPMS [Potts, 1987; Jenner and Arevalo, 2016], determining the proportion of Fe^{2+} requires wet chemical oxidative volumetric or complexiometric titrations (Wilson, 1955; Saikkonen and Rautiainen, 1993; Potts, 1987). Most igneous rocks and many other crustal rocks (Zen 1985) sit near FMQ or at slightly more oxidized conditions, which are towards the Hematite-Magnetite oxygen buffer (Fudali, 1965; Carmichael and Nicholls, 1967, Clark, 1997) while mantle rocks, particularly in the garnet peridotite stability field, tend to be marginally lower than FMQ (McCammon and Kopylova, 2004).

Most of the crust is igneous and the primary minerals derive from cooling and crystallization. Embedded in the other various processes that comprise the rock cycle are redox changes which either make rocks more reduced or more oxidized depending on which minerals fractionate and what fluids are present (Sossi et al., 2012). Most subsequent geological processes following igneous crystallization, including: deuteric alteration, oxidation, hydration, weathering, sedimentary transport, sedimentary deposition, metamorphism, hydrothermal alteration, sulfidation, and ore formation, increase or reduce oxygen fugacity and destroy primary magnetite; thereby leading to a reduction in magnetic susceptibility. On the Henkel plot, the magnetite trend marks where magnetite occurs in maximum proportions to other minerals due to the FMQ buffer. The more reduced magnetite-wustite buffer has more ferrous iron than can be accommodated by magnetite, so more of the iron forms FM silicates with lower susceptibility. The more oxidized magnetite-hematite buffer has more ferric iron than can form magnetite, so it forms some hematite instead and thus has lower susceptibility. If oxygen fugacity were to be plotted perpendicular to the usual susceptibility-density plane for the Henkel plot, the magnetite trend would actually form a high saddle that falls off both directions away from this plane (Fig.7).

Because of its abundance and two common valences, it has long been recognized that iron as an element has two rather different modes of chemical behaviour (Goldschmidt, 1937). Ferrous iron is the most abundant form and it tends to be soluble in natural waters and igneous melts. Ferric iron tends to form insoluble residues chiefly as oxy-hydroxides. Thus at higher fO_2, hematite or other less susceptible ferric oxy-hydroxides form at the expense of magnetite (e.g., subaerial weathering, gossans, soil formation). Lower fO_2 destroys magnetite and forms ferrous silicates during metamorphism, or solvates and removes iron from the system altogether. In subaqueous deposition of sediments, water is an oxygen barrier. This barrier and the tendency for bacteria to consume any buried organic matter, progressively reduces sediments as a function of burial depth. This reduction consumes any Fe^{3+} in magnetite or oxidized silicate minerals (to form ferrous silicates), while reducing any dissolved sulfate in pore waters to sulfide (Malinverno and Pohlman, 2011, Pohlman et al., 2013). In hydrothermal and other ore forming environments within the crust, lower fO_2 and high fS (sulfur fugacity as S^{-2}, HS^{-}, etc.) mainly produces Fe^{2+} sulfide minerals (pyrite, pyrrhotite, chalcopyrite, sphalerite, etc.) at the expense of magnetite. With the exception of pyrrhotite, formation of these sulfide minerals also serves to lower the bulk magnetic susceptibility during sulfide ore formation.

5.1 Igneous Rocks

Most of the crust and the entire mantle is composed of igneous rocks. Bowen's Reaction Series (Bowen, 1922) describes the ordinary sequence of crystallization of primary igneous minerals as a function of falling temperature. The predominant processes governing these igneous minerals and the rocks they form include: crystallization as a function of falling temperature, fractional crystallization, reaction with residual melts as magmas cool in place, and contamination during intrusion or emplacement through the crust. Mg^{2+} and Fe^{2+} ions have similar size, so they substitute in the same minerals. Mg^{2+} is slightly smaller, so it forms stronger bonds and tends to crystallize first at higher temperature into ferromagnesian silicates. The discontinuous reaction series – olivine, pyroxene, amphibole, biotite – involves the early high temperature crystallization of FM minerals, rich in Mg^{2+} and Fe^{2+}, which react with the silicate melt as the melt cools and further polymerizes. Magmas, and igneous rocks derived from them, become progressively depleted in Mg^{2+} and enriched in Fe^{2+} as these earlier ferromagnesian minerals crystallize and are fractionally removed during further magma ascent. Therefore, most FM minerals are more Mg-rich than ferrous and the partitioning of Mg and Fe between coexisting pairs of minerals acts as a kind of geothermometer (Brown and Vincent, 1963; Carmichael, 1967; Bhattacharya et al., 1992; Loucks, 1996; Ravna, 2000).

Magmas fractionate as they crystallize, thus ferromagnesian-enriched minerals tend to be denser than the magmas they came from and therefore they settle as crystal aggregates. Removal of FM enriched phases leads to progressively enhanced concentration of silica, water, alkalis and minor elements in the residual magma (Irvine and Baragar, 1971). Clark (1999) figure 7 using data reported by Puranen (1989), and Enkin (2018) figure 18 show a systematic decrease in density and susceptibility with ordinary igneous fractionation through the series: gabbro – diorite – quartz diorite – granodiorite – granite.

To a first approximation, the abundant minerals which control rock density do so by having a few percent minerals with some heavier Fe content in their composition. Oceanic crust is predominantly basalt or gabbro with total iron oxide content <15% by weight and about half of their volume as the ferromagnesian silicates olivine and pyroxene. These minerals crystallized at high temperature and selectively took up smaller Mg ions rather than larger ferrous iron, giving them densities at the low end of the range for those minerals (olivine-3.32 g/cm^3, augite-3.40, hypersthene-3.55). Continental crust is predominantly granite and granodiorite having less than 15% by volume of hydrated ferromagnesian silicates with somewhat lower densities (hornblende-3.23, biotite-2.94) owing to less net iron, more silica and more of lighter elements like Na or K with higher coordination volumes.

As most igneous magmas, and the rocks they generate, evolve in the crust via cooling and crystallization, they tend to remain in the FMQ oxygen fugacity buffer (Carmichael, 1967; Kress and Carmichael, 1991). Ferric iron does not fit in most common rock-forming QFC or FM minerals, so it crystallizes as iron oxides. Once magnetite starts to crystallize on cooling, it removes the Fe^{3+} preferentially. Thereafter, FM mineral fractionation follows the FMQ buffer as magnetite and ferrous ferromagnesian silicate minerals continue to crystallize (Fudali, 1965; Carmichael and Nicholls, 1967). Furthermore, at magmatic conditions of $-8 < \log_{10}(fO_2 \text{ atm}) < -6$ and 1200°C to 1000°C typical basalts have an atomic ratio of ferrous to total iron $Fe^{2+}/(Fe^{2+}+Fe^{3+}) \sim 0.65$ while granodiorites are a bit lower at ~0.58. The fractional crystallization process produces a predominance of ferrous ferromagnesian silicate (FM) minerals along with subordinate magnetite in both volcanic and plutonic igneous rocks (Middlemost, 1989).

Essentially all the Fe^{3+} is incorporated into magnetite as long as Fe_2O_3 is less abundant than FeO in a molecular sense (or ferrous iron is greater than one third of total iron). At higher oxygen fugacity, a combination of magnetite and hematite forms. The maximum amount of magnetite is formed when $Fe^{2+}/(Fe^{2+}+Fe^{3+}) \sim 0.35$. The precise ratio depends on the other elements present in the melt. At this maximum, every percent iron by weight produces about 0.5% magnetite by volume. It is very rare that a mafic magma will contain more than 15% iron, so even at optimal oxidation, magnetite content in igneous rocks can rarely be above 8%. In the CRPPD (Enkin, 2018), only 2% of plutonic rocks have magnetic susceptibility above $7.6 \cdot 10^{-2}$ SI (that is, 2.5% magnetite by volume) and 2% of volcanic rocks have magnetic susceptibility above $5.9 \cdot 10^{-2}$ SI (that is, 2.0% magnetite).

Most of the natural variation in magnetite concentration is not due to variation away from the FMQ buffer itself but due to the influence of other elements (Mg, Ti, Na, K, etc.) on the size and position of the magnetite stability field in temperature-fO_2 space (Frost and Lindsley, 1991; Clark et al., 2003). Essentially the addition of Mg (as in more mafic magmas) raises fO_2 of the Olivine-Magnetite-Quartz buffer compared to pure FMQ because Mg preferentially enters olivine compared to magnetite and enters magnetite compared to hematite. This is sensible because ordinary differentiation drops the Mg number and magnetite crystallization is limited to higher oxygen fugacities (Clark et al., 2003). Conversely, Ti is preferentially taken up by ulvospinel ($Fe^{2+}TiO_4$) instead of Fe^{3+} as magnetite in the cubic phase, or ilmenite ($Fe^{2+}TiO_3$) instead of hematite in the hexagonal phase. Hence, the addition of Ti (as in more alkaline or evolved Fe and Ti enriched magmas) tends to drop both the FMQ and HM buffers to lower fO_2. In strongly alkaline melts, the excess alkalis are taken up by ferrous alkali ferromagnesian minerals such as acmite, aegerine or riebeckite, which in turn reduces the stability fields and crystallization for both magnetite and hematite (Platt and Woolley, 1986).

The related set of points on the Henkel plot follows the magnetite trend from the high density and high susceptibility mafic rocks (derived from hotter magmas with higher CI) progressing to lower density and lower susceptibility felsic rocks (derived from cooler residual magmas). The mode, or most populated point, of the magnetite trend (2.66 g/cm^3, $1.9 \cdot 10^{-2}$ SI) is representative of granite, the most common continental crustal rock. Granite composition is so common because it forms at the granite eutectic minimum (quartz, alkali feldspar, plagioclase) on the composition-temperature graph (Bowen, 1922), that is, the low temperature residue composition for either the end of magma cooling and crystallization, or the common starting composition for beginning of partial melting (anatexis) on rock heating and ultra-metamorphism (Sawyer et al., 2011).

The existence of unaltered volcanic rocks which carry atypically low magnetic susceptibility ($\sim 10^{-3}$ SI), such as the Miocene Chilcotin basalts of central British Columbia (Enkin, 2014), helps test our model justifying the predominance of volcanic rocks with susceptibilities above 10^{-2} SI lying on the Henkel plot Magnetite Trend. The Chilcotin Basalts are within-plate, dry, glassy, mafic, olivine bearing volcanic rocks (Dostal et al., 1996, Bevier, 1983). They have low magnetic susceptibility because, with low water initial content, the primary ferrous minerals and glassy groundmass was preserved and iron was trapped in volcanic glass, rather than forming the equilibrium concentration of magnetite that would be expected from the equivalent plutonic gabbros. The reduced oxidation state typical of the lower crust was preserved through the passage to the surface because the dry magma did not allow equilibration with the surrounding crustal rocks or fluids.

5.1.1. Density – Magnetic Susceptibility Model Verification from Geochemistry and CIPW Norms

Igneous rocks are classified by their modal mineral proportions or their chemical composition. Visual estimate of the modal colour index (CI = proportion of dark FM silicates) of coarse-grained plutonic rocks and even microcrystalline volcanic rocks is possible for hand specimens and thin sections. A problem arises in attempting to classify very fine grained or glassy volcanic rocks when there are few phenocrysts. This problem was addressed by Cross et al. (1902) to calculate a norm (that is, mineral proportions derived from chemical composition) to analyse and classify volcanic rocks based on their bulk chemical composition. The CIPW Norm, named after its original developers: Cross, Iddings, Pirsson, and Washington (Johannsen, 1931), still serves with little modification (Johannsen, 1931). The CIPW norm calculation assigns the elemental analytes to minerals, as if the rock were fully crystallized as per intrusive plutons. This type of calculation permits a chemical analysis to be recast as mineral proportions. It is particularly useful where chemical analyses have been performed but the rock has not been analysed for its constituent minerals by visual or microscopic techniques. In common non-peralkaline igneous rocks (Middlemost, 1989), every 2 ions of Fe^{3+} take one ion of Fe^{2+} to form magnetite. If rocks are oxidized, not fresh, or have not been analysed for the ferric iron component, some correction must be made, or inappropriate values will be estimated for hematite, quartz, and orthopyroxene. Given these types of corrections to primary Fe^{2+}/Fe^{3+} ratios, the chemistry may be used quickly and accurately to provide normative estimates of CI to correctly assign rock names. These calculations are so robust, that within broad assignments of iron oxidation states, reasonable normative estimates of QFC-FM-M mineral proportions, and thus CI, density and magnetic susceptibility are obtained.

CIPW norms for igneous rocks were calculated individually using a spreadsheet program (Hollocher, 2004) and for groups of related rocks using other programs such as those in IOGAS, to provide a check on our three-component model classification for the density and magnetic susceptibility values on the calibrated Henkel petrophysical plot. If our petrophysical model is valid then it should be possible to estimate density and susceptibility values from chemical analyses. To test this suggestion, we chose fresh unaltered volcanic rocks that span the majority of common igneous rock types, specifically a rhyolite Newberry volcano (Kuehn and Foit, 2006) and a Galapagos ferrobasalt differentiate (Clague and Bunch, 1976). The M proportion is simply the CIPW estimate volume percent of magnetite. The QFC proportion is the sum of quartz, orthoclase, and plagioclase proportions in saturated igneous rocks or nepheline in undersaturated ones. The FM proportion is the sum of ferromagnesian silicates: olivine, orthopyroxene, diopside, plus a few dense, less-magnetic minerals (ilmenite, hematite, apatite, corundum) indicated with square brackets on Figure 2. While these non-silicate minerals are rare, they are included because they have density and susceptibility values similar to the FM silicates in our calibrated model for the Henkel plot. The theoretical density of the whole rock was calculated from the volume percentages of the end member norm minerals and their density values. The CIPW estimate of magnetic susceptibility is 3.0SI/100% times the volume percent of magnetite. As discussed above paramagnetic mineral contribution to total susceptibility is limited to less than 3×10^{-4} SI, or less than 0.03% Magnetite content. We used $Fe^{2+}/(Fe^{2+}+Fe^{3+}) = 0.65$ as the oxidation state but varied the ratio to verify how robust the results are to oxidation state.

The derived density and magnetic susceptibility values for the rhyolite plotted near the mode for the magnetite trend in the CRPPDB (2.66 g/cm^3, $1.5 \cdot 10^{-2}$ SI). The ferrobasalt was

chosen as an extreme case, having a total FeO* value of 16.97%. As such its density and susceptibility values plotted far along the upper magnetite trend at (3.12 g/cm^3, 1.73·10^{-1} SI). Varying the oxidation state only changes the density by up to ±0.5%, while the susceptibility is robust to a factor 2 up of down.

5.2 Sedimentary Rocks and Processes

Most sedimentary rocks are characteristically of low magnetic susceptibility and low density. Sedimentary rocks contain only trace amounts of magnetite, and the low density reflects the common sedimentary minerals (quartz, feldspar, clays, and carbonates) and their inherently high porosity. Potential field methods tend to see through sedimentary cover sequences and instead respond to the more deeply buried underlying igneous and metamorphic basement rocks. Where thick accumulations of sediments and sedimentary rocks occur they make lows on both gravity and magnetic maps. The small amount of magnetite and iron places sedimentary rocks on the paramagnetic trend on the Henkel plot (Fig.3, yellow points).

Liquid water present at the surface of the earth, and as subsurface ground water, is active in removing magnetite from rocks during weathering, transport and diagenesis, as indicated by the black arrow in Figure 7. Water acts as a chemical weathering agent by hydrating the surface of minerals, hydrolyzing minerals and replacing some of their exposed surface cations with hydrogen ions, and dissolving minerals to remove mineral matter as solutes. Ferrous iron in minerals, including ferromagnesian silicates, carbonates, magnetite, pyrite and other ferrous sulfides, is preferentially soluble. Depending on the chemical environment, iron may be partially retained as clay minerals and oxy-hydroxides, but usually it suffers some net loss via dissolution and leaching, to the point that most sediments are iron poor. Sedimentary residues tend to comprise quartz, clay minerals, aluminous oxy-hydroxides, or reprecipitated soluble phases such as calcite, gypsum and other salts.

Sedimentation on land occurs in the presence of atmospheric oxygen, acidic rain or fresh oxidized surface waters. These conditions leach iron from the rocks and oxidize ferrous ions to ferric ions, thus transforming magnetite to hematite or to ferric iron oxy-hydroxides (goethite or limonite), thus decreasing the magnetic susceptibility (Lapointe et al., 1986) as indicated by the red arrow in Figure 7. As iron oxides are often the dominant pigments in rocks, red and yellow rocks usually indicate that their iron has been leached, oxidized, and deposited as fine-grained pigments and films coating mineral surfaces. Rapid oxidation of pyrite, pyrrhotite or other ferrous iron bearing sulfide minerals causes sedimentary materials which contain them to generate ferrihydrite, goethite, or hematite by-products as a characteristic feature of acid rock drainage generated from exposed sulfide minerals or mine tailings (Shang et al., 2009). As a by-product of the oxidizing sulfuric acid generated from acid rock drainage, weathering and removal of ferrous iron from primary magnetite and ferromagnesian silicate minerals is enhanced so magnetite content is diminished by these acid leaching and oxidation processes as well.

In anoxic conditions, primary magnetite rich sediment can be preserved. Pozza et al. (2004) mapped the distribution of magnetite-rich contaminated sediments in the Randle Reef area of Hamilton Harbour. The presence of bacteria in the water column and shallow pore waters plus any organic content serves to scavenge oxygen and reduce ferric iron (Fe^{3+}), so magnetite is destroyed diagenetically (Grant, 1985a), as indicated by the green arrow in Figure 7. In swamps, and deep basins with abundant organic content, the bacterial oxidation of organic matter not only consumes free dissolved oxygen, but also steals oxygen from oxy-anion solutes

(nitrate, sulfate etc.) (Malinverno and Pohlman, 2011; Pohlman et al., 2013). Under such anoxic organic-rich conditions, the presence of any oxidized iron in detrital magnetite is also bacterially reduced producing fully reduced pyrite if sulfur is not limiting or temporary environmental iron sulfides where it is limited (Hamilton et al, 2010; Esteban et al., 2010).

Volcaniclastic rocks, immature lithic sediments containing plutonic, volcanic or metamorphic lithic fragments and placers from continental sediments and sedimentary rocks, contain sufficient primary magnetite (Parker et al., 1991) that they tend to plot along the magnetite trend on the Henkel Plot (Fig.3). The other rare but notable sedimentary rock exceptions which plot at high density and susceptibility are placer deposits and banded iron formations (Klein, 2005). Note that the two or more orders of magnitude between the magnetite and paramagnetic trends on the Henkel plot suggests that it takes the magnetite leached from at least 1000 volumes of rock to concentrate into one volume of sedimentary magnetite placer or chemical ironstone.

5.3 Metamorphic Processes

There are relatively few common bulk compositions or rock types (Wyllie, 1971) for regional metamorphism, since there are few dominant protoliths: pelites (mud rocks, ~80% of sediments), psammites (sandstones), volcanics (dominantly mafic basaltic seafloor or intermediate andesites from primitive volcanic arcs) or plutonics (dominantly granites to granodiorites). In continental shields and uplifted orogenic belts, these protoliths tend to produce regionally extensive dynamo-thermal metamorphic rocks such as schists, greenstones, amphibolites or gneisses.

Prograde metamorphism tends to be buffered by the mineral assemblage (Eugster, 1957) and thus tends to preserve the predominant fO_2 series along the FMQ oxygen fugacity buffer like their protoliths, especially for igneous assemblages (Grant, 1984a). In the rare case of abundant hematite in the sedimentary protolith, prograde metamorphism can produce some magnetite but more generally it is destructive of magnetite by favouring the preferential production of ferrous silicates. Thus, metamorphic processes usually place rocks on the paramagnetic trend on the Henkel plot (Fig.3), after having followed the magnetite-loss black arrow in Figure 7.

Prograde metamorphism involves heating via burial down the geothermal gradient during plate collision and mountain building (Barrovian style metamorphism) or via increases in the geothermal gradient such as occurs above or next to crustal intrusions in volcanic arcs, along rifts or near within-plate plutons (such as Buchan style metamorphism or contact metamorphism). Most prograde metamorphism involves fluid loss, desilication and densification and rates of these reactions are geologically rapid (Walther and Wood, 1984). The typical prograde metamorphism releases fluids during dehydration and decarbonation reactions along with some soluble silica and cations being driven off metasomatically to shallower and cooler levels of the crust. There is a tendency, due to Mg^{2+} being slightly smaller than Fe^{2+}, for iron to dissolve and leave with the fluids. The maximum temperature is recorded within the highest-grade mineral assemblage via increases in Mg/Fe ratios for the FM silicate minerals. This is tantamount to moving the rock back up Bowen's discontinuous reaction series, for example:

$$\text{Biotite} \rightarrow \text{Hornblende} + H_2O + SiO_{2\,aq} + Fe^{2+}_{aq} \quad , \qquad \text{[eq. 10]}$$

and so on for the formation of pyroxene or olivine instead of amphibole. Depending on buffering by ferromagnesian minerals, fO_2, and other elements, magnetite may be created (Grant,

1984a) or more often consumed, especially if ferrous iron is lost to the system along with expelled fluids. This process leaves more Mg-rich greenstone or amphibolite residues, or rocks with iron forming ferrous silicates: garnet, staurolite, epidote, chlorite, chloritoid etc., which are notably lower in magnetic susceptibility than when part of the iron was ferric and contained within magnetite in their protoliths. Along with increasing Mg/Fe ratios in prograde metamorphism, alkalis (Na, K) are selectively driven off during prograde dehydration reactions. Thus, igneous or immature clastic sedimentary protoliths having primary feldspars, leave more aluminous and calcic, denser metamorphic mineral residues as the larger and higher coordination number cation sites in framework or sheet silicates are lost. The metamorphic fluids are less dense than the rocks undergoing heating and burial, so they escape to shallower levels of the crust and carry some silica, salts, and iron to mineralizing or ore-forming settings higher up in the crust. Collectively these processes tend to produce denser, less magnetic, prograde residual metamorphic rocks than their protoliths.

There is a tendency for an increase in susceptibility for higher grade metamorphic rocks in the upper amphibolite and granulite facies (Grant, 1984a). This is due to making progressively more magnesian-rich ferromagnesian silicates and putting Ti and Fe back into titanomagnetite as grade and temperature increase.

Rock becomes denser during burial and compression down the geothermal gradient because they are squeezed faster than they are heated (most minerals are insulators for heat conduction). As minerals are compressed, they recrystallize to denser forms and denser configurations with less void space by sharing some edges (2 shared oxygens between adjacent polyhedra, not just one). While the Fe content principally governs their density and magnetic susceptibility, in higher pressure metamorphic environments Al can also exert an influence on rock density. Al^{3+} is a small cation which sits in either tetrahedral or octahedral sites surrounded by oxygen. With increasing pressure, the size of the oxide ion decreases producing two consequences. Higher pressure also favours the smaller tetrahedral-Al sites so in some mineral assemblages this partitioning can serve as a geobarometer as noted for hornblende calc-alkaline and metaluminous igneous rocks (Hammarstrom and Zen, 1986; Hollister et al., 1987; Johnson and Rutherford, 1989; Rutter et al., 1989; Mutch et al. 2016). Both tetrahedral-Al and octahedral-Al achieve slightly denser packing configurations as a function of pressure. There is also a tendency to reduce void space between polyhedral and for some edge sharing to occur which also decreases void space. Examples of denser Al-bearing minerals which form during higher pressure metamorphism include: garnet and staurolite, corundum, kyanite, and garnet with typical densities in the range of 3.6-4.5 g/cm^3, as per the minerals in red on Figure 2. All of these rock forming minerals in meta-pelites are denser than our selected FM end member so they can increase rock density in proportion to their presence and produce a shift in the Henkel plot envelope (Fig.6). For example, the increasing density with prograde regional metamorphism of a kaolinite-rich shale proceeds as: Kaolinite (2.60 g/cm^3) → Pyrophyllite (2.84 g/cm^3) → Andalusite (3.15 g/cm^3) → Kyanite (3.61 g/cm^3).

Retrograde metamorphism of mafic and ultramafic rocks, through the process of serpentinization, involves hydration and oxidation and results in products that are generally at odds with the outcome expected from more silica rich rocks (Adams and Dentith, 2016). This process is regionally significant because of the amount of serpentinized ultramafic rocks in accreted oceanic crust (Bonatti, 1976) and greenstone belts (Williams, 2009). First, increased serpentinization is associated with the mobility of several elements including iron (Peters et al.,

2017) and thus it is generally accompanied by a gradual reduction in the observed density (Dentith and Mudge, 2014) and an increase in susceptibility (Williams, 2009), in marked contrast with the generally low magnetic signature of greenstone belts compared to granitoids (Grant 1984b) due to loss of magnetite and iron during more typical prograde metamorphism. Toft et al. (1990) attribute this reduction in density to the hydration and formation of hydrous sheet minerals like brucite and talc at the expense of denser FM silicates, along with an increase in porosity. Magnetization increases with the degree of serpentinization because hydration and oxidation destroy primary olivine and produce secondary magnetite as ferrous iron is released and oxidized (Peters et al., 2017). Malvoisin et al., (2012) report a linear relationship between magnetite production and the serpentinization process. For this specific class of rocks, metamorphism can move samples further towards the magnetite trend but with reduced density (Williams, 2009). Representative reactions would be the consumption of olivine to produce brucite, quartz (or soluble silica lost to the system) and magnetite:

$$3\ MgFe^{+2}SiO_4 + 3\ H_2O + ½\ O_2 \rightarrow 3\ Mg(OH)_2 + 3\ SiO_2 + Fe^{+2}\ Fe^{+3}{}_2O_4\ ,\quad \text{[eq. 11]}$$

or the production of talc and magnetite from olivine and fluids with aqueous silica:

$$3\ MgFe^{+2}SiO_4 + SiO_2 + H_2O + ½\ O_2 \rightarrow 3\ Mg_3Si_4O_{10}(OH)_2 + Fe^{+2}\ Fe^{+3}{}_2O_4\ .\ \text{[eq. 12]}$$

Ultramafic rocks typically have much higher Mg/(Mg+Fe) ratios, generally between 0.8 and 0.93, rather than 0.5 as indicated by these reactions for an intermediate olivine. In all cases there is a very high water/rock ratio, greater than 1000/1, accompanying the recrystallization, so these systems are open and involve bulk changes to the chemical composition (Peters et al., 2017). Structurally these serpentinites tend to be associated with faults which provided the fluid conduits and petrographically the primary olivine and pyroxene are replaced by serpentine or talc pseudomorphs with inclusions of pure, low-temperature, magnetite or chromite.

5.4 Mineralization Processes

Mineralization processes associated with deposition or removal of magnetite have been reviewed by Grant (1984b) and Clark (2014). Grant (1984b) presents the case for stratigraphic and structural ore associations. In terms of stratigraphic associations, magmatic style mineralization is associated with “a) thick sequences of calc-alkaline volcanics, b) the presence of ultramafic flows, c) acidic pyroclastic sequences and d) overlying chemical sediments.” Under structural concepts, the quantity of magnetite is dependent upon the nature of the fault generation process and the chemistry of the fluids that migrate through the fractures. Grant presents three options: a) carbonate rich solutions where any magnetite present will be converted to less magnetic siderite, b) saline solutions carrying iron chlorides that lead to deposition of magnetite around brine vents, 3) silica rich solutions which are oxidising and lead to destruction of magnetite and generation of magnetic anomaly lows associated with fracture systems as described by Henkel and Guzman (1977). It must be noted though that not all faults are associated with broad alteration zones. In some instances, it is possible to find lateral displacement of a distinctive magnetic anomaly across a fault boundary that is not associated with a localized alteration zone.

Sulfur (row 3 of the periodic table) only occurs in about 0.2% of most crustal rocks and makes sulfide or disulfide or sulf-arsenide ions, which are significantly larger than oxide ions (row 2). As a result while there are slightly magnetic Fe-bearing sulfide minerals: bornite, sphalerite, ferroan chalcopyrite etc., the iron in those minerals sits farther apart and the net

magnetization is less than with the tighter spacing as oxides. Deposition of magnetite, or magnetic sulfide mineral such as pyrrhotite, is controlled by oxygen fugacity – temperature relationships in the Fe-S-O system. As shown by Grant (1984b, Figure 3) when metal rich brines (black smokers) associated with volcanic vents mix with sea water the resulting mineralization sequence is controlled by change in temperature and pH. The first mineral to be deposited will be pyrrhotite and then magnetite, however, in the presence of increased sulfur or lowered pH, only limited amounts of magnetite will be deposited.

Clark et al., (2003) developed the concept of predictive magnetic exploration models for porphyry copper and IOCG deposits. The basis of this concept is that these types of deposits have similar magnetic signatures as a result of having common tectonic setting, and magma association. However, details of the magnetic signature might vary with depth of burial, or post-emplacement faulting of the mineral deposit. Clark (2014) Table 2 presents a list of the characteristic alteration systems and mineral assemblages that can form along with porphyry copper deposits. Early crystallization from a parental magma is commonly accompanied with enhanced presence of magnetite. Subsequent and progressive alteration, including the formation of potassic, sericitic, and argillic phases, produce increased levels of magnetite destruction such that the presence of mineralization is commonly associated with the most-weakly magnetised part of the intrusive system. When intermediate magmas intrude limestones for various chemical reasons, strongly magnetic skarns form along the contact.

IOCG deposits are commonly characterized by positive magnetic and gravity anomalies. Typically, IOCG deposits are associated zones which formed from high concentrations of iron-rich fluids. Sodic and sodic-calcic alteration zones in these settings may extend over tens to hundreds of square kilometers. These metasomatic fluids also tend to be carbonate rich. All of these factors lead to an increased association of magnetite with these types of deposits. Enkin et al. (2016) studied the NICO IOCG deposit associated with the Great Bear Magmatic Zone. There, the mineralization is generated through the migration of a sequence of fluids starting with 1) albitization from hot deeply derived sodic fluids, followed by 2) calcium metasomatism with the creation of amphibole, and iron-rich metasomatism creating magnetite which produced the highest densities and magnetic susceptibilities, and finally a 3) potassic alteration with the creation of K-feldspar and the destruction of magnetite producing lower densities and susceptibilities. Note that much of the IOCG mineralization is associated with this third metasomatic facies, thus explaining the common association of mineral deposits adjacent to magnetic and gravity highs (Clark, 2014).

6 Example

Many of the concepts we have just described are clearly at play in the Henkel plot of samples collected from the Highland Valley Copper deposit of south-central British Columbia, Canada (Fig. 8), as part of the Canadian Mining Innovation Council and Canadian National Science and Engineering Council Footprints Project. This porphyry deposit sits within the Early Jurassic Guichon Batholith, which presents as a series of concentric shells, where the outer early shells are mafic and became progressively more felsic towards the centre as the plutonic system evolved (Byrne et al., 2019, Lesage et al., 2019, Vallée et al., 2019a). The densities and magnetic susceptibilities of the unaltered, least altered and weakly altered samples (diorite to granite) clearly plot along the magnetite trend. As reported in Vallée et al (2019a, Figure 3 and Table 1), the average susceptibility of batholith's phases decreases systematically from the more mafic

outer Border Phase, through the Guichon, Chataway, Bethlehem, Skeena, to the more felsic inner Bethsaida Phase. The strong magnetic contrast between the arithmetic mean susceptibility of the outer Border and Guichon phases and the less magnetic country rock and the inner more felsic phases (one order of magnitude) leads to the generation of a significant magnetic anomaly which has been modeled to define the 3D geometry of the outer shell of the intrusion (Vallée et al., 2019a). Density values also exhibit a similar trend with higher values (2.80 g/cm^3) being associated with the more mafic Border Phase to values around 2.66 g/ cm^3 being associated with the most felsic Bethsaida Phase (Vallée et al., 2019b, Figure 12). Unfortunately, this minimal variation in density contrast together with limited gravity observations means that the gravity anomaly associated with the pluton defines a broad negative anomaly. Nonetheless, constraining a 2.5D model with Lithoprobe seismic bounds, Roy and Clowes (2000) were able to demonstrate that Guichon pluton has the broad form of a funnel shaped intrusion with the main mineralised zone being located above the “stem” (deep feeder zone) of the batholith. Using density values reported by Ager et al., (1973) the best-fit gravity profile model calculated by Roy and Clowes (2000) included a contrast of -0.15 g/cc between the outer more mafic units and the inner more felsic phases. Using the same geologically and seismically constrained approach on a more recent airborne gravity dataset gave more consistent coverage but with less detail (Vallée et al., 2019b). Using this low resolution airborne gravity data, they were able to define a sharp western margin of the batholith, but their inversion was unable to detect any internal structure of the pluton.

Hydrothermal alteration is prevalent throughout the Guichon Batholith leading to a decrease in magnetic susceptibility as shown in Figure 8. As the level of alteration increases the susceptibility values more closely approximate the “Paramagnetic” Trend. Using a cumulative probability plot Vallée et al. (2019a, Figure 3) show that the more felsic rocks have a higher degree of alteration than the outer more mafic phases. Henkel and Guzman (1977), using petrophysical measurements, linked linear negative magnetic anomalies to alteration associated with fracture zones. Increased flow of shallow crustal, oxygen rich fluids along the fault zones lead to progressive oxidation of magnetite to less magnetic phases. By extracting profiles across the negative magnetic anomalies, and modeling the feature as a dipping prism, Lesage et al., (2019) were able to construct a 3-dimensional structure of the brittle deformation within the Guichon Batholith. Each fracture system produced its own zone of alteration. Using this observation allowed Byrne et al. (2019) to use magnetic susceptibility, especially its dispersion at the outcrop scale, to map the progressive increase in alteration associated with an increased fracture density and increased fluid flow with proximity to each mineralised zone.

7 Conclusions

The Henkel petrophysical plot has utility for distinguishing lithologies and characterizing geological processes that is complementary to several popular geochemical plots (AFM, TAS, etc.). The typical locations, in density versus magnetic susceptibility space, for the dominant crustally significant rock types has been indicated by Henkel and others on the Henkel plot (Henkel, 1976, 1991, 1994, Williams, 2009). We corroborate this, and provide a version based on lithologies compiled in the Canadian Rock Physical Property Database in Figure 9. Igneous rocks fall on the magnetite trend, from mafic types with higher density and magnetic susceptibility to felsic types at lower density and susceptibility. Most regional metamorphic rocks plot along the paramagnetic trend due to iron reduction and fluid losses during prograde metamorphism. Sedimentary rocks, except for immature volcaniclastic rocks, fall on the

paramagnetic trend, with the clean carbonates and siliciclastics plotting down at the lowest magnetic susceptibilities. Rocks with significant porosity such as vesicular volcanics, porous sedimentary rocks, k-feldspar rich arkoses and clay-altered rocks can have densities below the QFC density of ~2.6 g/cm^3. Oxides and sulfides in mineralized rocks raise the density of rocks above the FM density of ~3.2 g/cm^3 as per Figures 2 and 6. By calibrating the Henkel petrophysical plot in terms of the 3 common rock forming mineral groups: QFC, FM and M, one can readily estimate the colour index (FM versus QFC) and magnetite content. Furthermore, the additional calibration examples of introducing denser sulfide (pyrite, sphalerite and pyrrhotite) and silicate (garnet) mineral phases helps to interpret atypically dense rocks which fall off the main magnetite and paramagnetic trends (Fig. 6). These mineral calibration models prove useful to geophysical data inversion for the interpretation potential field maps in a variety of geological settings and areas with economic ore deposits. Additionally, the disposition of related suites of rocks on this petrophysical plot can also be used to infer geological processes such as oxidation, sulfidation and alteration as an aid to the interpretation and integration of more detailed geophysical mapping and geological sampling.

Rocks comprise mineral assemblages with various textural relationships due to one or more geological processes that created them. Not all rocks result from equilibrium assemblages of well-crystallized minerals. Specifically, the disposition of the iron between ferrous and ferric ions, and silicates versus oxides introduces considerable variation. Because of this, rocks which classify the same have some spread on the Henkel petrophysical plot. Also, rocks with fundamentally different minerals and origins can have very similar physical properties. This is neither a failure of classification schemes nor a result of errors in physical properties measurements but an intrinsic variability of these complex rock systems. Despite this non-uniqueness, calibrating the Henkel petrophysical plot in terms of three common rock-forming mineral groups serves to simplify the inversion and geological interpretation of geophysical data.

Data

All data presented in this paper are available in the Geological Survey of Canada, Open File 8460 (Enkin, 2018).

References

Adams, C., & Dentith, M. (2016). Towards an Understanding of the Effects of Alteration on the Physical Properties of Mafic and Ultramafic Rocks. ASEG Extended Abstracts, 1, 1-6, doi: 10.1071/ASEG2016ab28

Ager, C.A., Ulrych, T.J., & McMillan, W.J. (1973). A gravity model of the Guichon Creek Batholith, south-central British Columbia. Canadian Journal of Earth Science, 10, 920-935.

Airo, M-L. ed. (2015). Geophysical signatures of mineral deposit types in Finland. Geological Survey of Finland, Special Paper 58, 144p.

Aydin, A., Ferre, E.C., & Aslan, Z. (2007). The magnetic susceptibility of granitic rocks as a proxy for geochemical composition: Example from the Saruhan granitoids, NE Turkey. Tectonophysics, 441, 85-95.

Balsley, J.R., & Buddington, A.F. (1958). Iron-titanium oxide minerals, rocks, and aeromagnetic anomalies of the Adirondack area, New York. Economic Geology, 53(7), 777–805. doi: https://doi.org/10.2113/gsecongeo.53.7.777

Barth, T.F.W. (1948). The distribution of oxygen in the lithosphere. Journal of Geology, 56(1), 50-60.

Bevier, M.L. (1983). Implications of chemical & isotopic composition for petrogenesis of Chilcotin Group basalts, British Columbia. Journal of Petrology, 24(2), 207–226, doi.org/10.1093/petrology/24.2.207

Biedermann, A.R. (2018). Magnetic anisotropy in single crystals: a review. Geosciences, 8(8), DOI:10.3390/geosciences8080302

Bleil, U., & Petersen, N. (1982). Magnetic properties, in Landolt-Bornstein Numerical Data and Functional Relationships in Science and Technology. Group V: Geophysics and Space Research; 1b, Physical Properties of Rocks, ed: Angenheisterp, G., 308-432, Springer-Verlag, New York.

Bhattacharya, A., Mohanty, L., Maji, A., Sen, S.K, & Raith, M. (1992). Non-ideal mixing in the phlogopite-annite binary: constraints from experimental data on Mg−Fe partitioning and a reformulation of the biotite-garnet geothermometer. Contributions to Mineralogy and Petrology, 111, 87. https://doi.org/10.1007/BF00296580

Bonatti, E. (1976). Serpentinite protrusions in the oceanic crust. Earth and Planetary Science Letters, 32(2), 107-113, https://doi.org/10.1016/0012-821X(76)90048-0

Bowen, N.L. (1922). The reaction principle in petrogenesis. Journal of Geology, XXX(3), 177-198.

Brown, G.M., & Vincent, E.A. (1963). Pyroxenes from the Late Stages of Fractionation of the Skaergaard Intrusion, East Greenland. Journal of Petrology, 4(2), 175–197, doi.org/10.1093/petrology/4.2.175

Byrne, K., Lesage, G., Morris, W.A., Enkin, R.J., Gleeson, S.A., & Lee, R.G. (2019). Variability of outcrop magnetic susceptibility and its relationship to the porphyry Cu centers in the Highland Valley Copper district. Ore Geology Reviews, 107, 201-217.

Carmichael, I.S.E. (1967). The Mineralogy of Thingmuli, a Tertiary Volcano in Eastern Iceland., American Mineralogist, 52(11-12), 1815-1841.

Carmichael, I.S.E., & Nicholls, J. (1967). Iron-titanium oxides and oxygen fugacities in volcanic rocks. Journal of Geophysical Research, 72(18), 4665-4687, doi.org/10.1029/JZ072i018p04665

Carmichael, R.S. (1989). Magnetic Properties of Rocks. Chapter 4, Practical Handbook of Physical Properties of Rocks and Minerals, CRC Press, Bota Raton, FL.

Clague, C.A., & Bunch, T.E. (1976). Formation of Ferrobasalt at East Pacific Midocean Spreading Centers. Journal of Geophysical Research, 81(23), 4247-2456.

Clark, D.A. (1984). Hysteresis properties of sized dispersed monoclinic pyrrhotite grains. Geophysical Research Letters, 11(3), 173-176. https://doi.org/10.1029/GL011i003p00173

Clark, D.A. (1997). Magnetic petrophysics and magnetic petrology: aids to geological interpretation of magnetic surveys. AGSO Journal of Australian Geology & Geophysics, 17(2), 83-103.

Clark, D.A. (1999). Magnetic petrology of igneous intrusions: implications for exploration and magnetic interpretation. Exploration Geophysics, 30, 5-26.

Clark, D.A. (2014). Magnetic effects of hydrothermal alteration in porphyry copper and iron-oxide copper-gold systems: A review. Tectonophysics, 624-625, 46-65.

Clark, D.A., & Tonkin, C. (1994). Magnetic anomalies due to pyrrhotite: examples from the Cobar area, N.S.W., Australia. Journal of Applied Geophysics, 32, 11-32.

Clark, D.A., Geuna, S., & Schmidt, P.W. (2003). Predictive magnetic exploration models for porphyry, epithermal and iron oxide copper-gold deposits: implications for exploration. AMIRA Exploration and Mining Report 1073R, 398p. AMIRA International, https://wiki.csiro.au/confluence/download/attachments/457769088/Clark+etal+2004+P700+CSIRO+1073Rs.pdf)).

Clark, D.A., French, D.H., Lackie, M.A., & Schmidt, P.W. (1992). Magnetic petrology: Application of integrated rock magnetic and petrological techniques to geological interpretation of magnetic surveys. Exploration Geophysics, 23, 65-68.

Cross, W., Iddings, J.P., Pirsson, L.V. & Washington, H.S. (1902). A quantitative chemico-mineralogical classification and nomenclature of igneous rocks. Journal of Geology, 10, 555-697.

Deer, W.A., Howie, R.A. & Zussman, A. (1997). An Introduction to Rock Forming Minerals, London. 2nd ed., 694p.

Deer, W.A., Howie, R.A., Zussman, A., Bowles, J. & Vaughan, D. (2011). Rock-Forming Minerals: Non-Silicates: Oxides, Hydroxides and Sulphides, Volume 5a, London.

Dentith, M., & Mudge, S.T. (2014). Geophysics for the Mineral Exploration Geoscientist. Cambridge University Press

Dentith, M., Adams, C., & Bourne, B. T. (2017). Petrophysics and Exploration Targeting: Best Practice and Applications. In: Wyche, S. & Witt, W.K eds. TARGET 2017. Perth, Australia: abstracts: Geological Survey of Western Australia, Record 2017/6, Accessed online from Geoconferences WA (geoconferences.org.au), 37-39.

Dentith, M., Enkin, R.J., Morris, W.A., Adams, C., & Bourne, B. (2019). Petrophysics and Mineral Exploration: A Workflow for Data Analysis and a New Interpretation Framework. Geophysical Prospecting, https://doi.org/10.1111/1365-2478.12882.

Dostal, J., Church, B.N., & Hamilton, T.S. (1996). The Chilcotin basalts, British Columbia (Canada): geochemistry, petrogenesis and tectonic significance. Neues Jahrbuch für Mineralogie – Abhandlungen Journal of Mineralogy and Geochemistry, 170, 2, 207-229.

Dunlop, D.J., & Özdemir, Ö. (1997). Rock Magnetism Fundamentals and Frontiers. Cambridge Studies in Magnetism Series. XXI, Cambridge University Press, Cambridge. 573p.

Enkin, R.J. (2014). The rock physical property database of British Columbia, and the distinct petrophysical signature of the Chilcotin basalts. Canadian Journal of Earth Sciences, 51, 327–338.

Enkin, R. J. (2018). The Canadian Rock Physical Property Database: first public release. Geological Survey of Canada, Open File 8460, 68p., https://doi.org/10.4095/313389

Enkin, R.J., Corriveau L., Hayward, N. (2016). Metasomatic Alteration Control of Petrophysical Properties in the Great Bear Magmatic Zone (Northwest Territories, Canada). Economic Geology, 111, 2073–2085.

Esteban, L., Hamilton, T. S., Enkin, R. J., Lowe, C., & Novosel, I. (2010). Ch. 13. Gas Hydrates and Magnetism: Surveying and Diagenetic Analysis. 197-216. In: Geophysical Characterization of Gas Hydrates. Eds., Riedel, M., Willoughby, E., & Chopra, S., Geophysical Developments Monograph 14, Society of Exploration Geophysicists, SeISBN: 978-1-56080-219-8, print ISBN: 978-1-56080-218-1, https://doi.org/10.1190/1.9781560802197.ch13

Eugster, H.P. (1957). Heterogeneous Reactions Involving Oxidation and Reduction at High Pressures and Temperatures, Journal of Chemical Physics, 26, 1760, https://doi.org/10.1063/1.1743626

Feinberg, J.M., Wenk, H.-R., Renne, P.R., & Scott, G.R. (2004). Epitaxial relationships of clinopyroxene-hosted magnetite determined using electron backscatter diffraction (EBSD) technique. American Mineralogist, 89, 462-466.

Feinberg, J.M., Scott, G.R., Renne, P.R. & Wenk, H.-R. (2005). Exsolved magnetite inclusions in silicates: Features determining their remanence behavior. Geology, 33(6), 513–516. doi.org/10.1130/G21290.1

Fleet, M.E., Bilcox, G.A., & Barnett, R.L. (1980). Oriented magnetite inclusions in pyroxenes from the Grenville Province. Canadian Mineralogist, 18, 89-99.

Frost, B. R., & Lindsley, D. H. (1991). The occurrence of Fe–Ti oxides in igneous rocks. In: Lindsley, D. H. (ed.), Oxide Minerals: Petrologic and Magnetic Significance. Mineralogical Society of America, Reviews in Mineralogy, 25, 433–486.

Frost, B. R., Lindsley, D. H. & Andersen, D. J. (1988). Fe–Ti oxide–silicate equilibria: assemblages with fayalitic olivine. American Mineralogist, 73, 727–740.

Fudali, F. (1965). Oxygen fugacities of basaltic and andesitic magmas. Geochimica et Cosmochimica Acta, 29(9), 1063-1075. Doi.org/10.1016/0016-7037(65)90103-1

Goldschmidt, V.M. (1937). The principles of distribution of chemical elements in minerals and rocks. The seventh Hugo Müller Lecture, delivered before the Chemical Society on March 17th, 1937, Journal of the Chemical Society, 1937, 655-673, doi/ 10.1039/JR9370000655

Grant, F.S. (1984a). Aeromagnetics, geology, and ore environments, I. Magnetite in igneous, sedimentary and metamorphic rocks: an overview. Geoexploration, 23, 303-333.

Grant, F.S. (1984b). Aeromagnetics, geology, and ore environments, II. Magnetite and ore environments. Geoexploration, 23, 335-362.

Gunn, P.J., & Dentith, M.C. (1997). Magnetic responses associated with mineral deposits. AGSO Journal of Australian Geology and Geophysics, 17(2), 145-158.

Haggerty, S.E. (1979). The aeromagnetic mineralogy of igneous rocks. Canadian Journal of Earth Sciences, 16, 1281-1293.

Hamilton, T. S., Esteban, L., & Enkin, R. J. (2010). Petrographic, geochemical and magnetic properties of carbonate rock formation and low temperature diagenetic alteration of

unconsolidated sediments accompanying the formation of gas hydrate deposits, Proceedings of the 14th Symposium on the Geology of the Bahamas and other carbonate regions, 107-130.

Hammarstrom, J.A., & Zen, E-an. (1986). Aluminum in hornblende: An empirical igneous geobarometer. American Mineralogist, 71(11-12), 1297–1313.

Harrison, R.J., Dunin-Borkowski, R.E., & Putnis, A. (2002). Direct imaging of nanoscale magnetic interactions in minerals. National Academy of Sciences Proceedings, 99, 16556-16561.

Heider, F., Zitzelsberger, A., & Fabian, K. (1996). Magnetic susceptibility and remanent coercive force in grown magnetite crystals from 0.1 um to 6 mm. Physics of the Earth and Planetary Interiors, 93, 239–256.

Henkel, H. (1976). Studies of Density and Magnetic Properties of Rocks from Northern Sweden, Pure and Applied Geophysics, 114, 235-249.

Henkel, H. (1991). Petrophysical properties (density and magnetization) of rocks from the northern part of the Baltic Shield. Tectonophysics, 192, 1-19.Henkel, H. (1994). Standard diagrams of magnetic properties and density—a tool for understanding magnetic petrology. Journal of Applied Geophysics, 32(1), 43-53. https://doi.org/10.1016/0926-9851(94)90008-6.Henkel, H., & Guzman, M. (1977). Magnetic features of fracture zones. Geoexploration, 15, 173-181.

Hollocher, K. (2004). CIPW Norm Calculation Program Geology Department, Union College.

Hollister, L.S., Grissom, G.C., Peters, E.K., Stowell, H.H., & Sisson, V.B. (1987). Confirmation of the empirical correlation of Al in hornblende with pressure of solidification of calc-alkaline plutons. American Mineralogist, 72(3-4), 231–239.

Hinze, W. J. (2003). Bouguer reduction density, why 2.67? Geophysics, 68(5), 1559-1560.

Hunt, C.P., & Moskowitz, B.P. (1995). Magnetic properties of rocks and minerals. In Ahrens, T. J. (ed.). Rock Physics and Phase Relations: A Handbook of Physical Constants, 3. Washington, DC: American Geophysical Union. 189–204.

Irvine, T.N.J., & Baragar, W.R.A. (1971). A guide to the chemical classification of the common volcanic rocks. Canadian Journal of Earth Sciences, 8(5), 523-548. https://doi.org/10.1139/e71-055

Jenner, F.E., & Arevalo, R.D. Jr. (2016). Major and Trace Element Analysis of Natural and Experimental Igneous Systems using LA–ICP–MS, GeoScience World Elements, 12(5), 311-316. DOI: 10.2113/gselements.12.5.311

Johnson, M.C., & Rutherford, M.J. (1989). Experimental calibration of the aluminum-in-hornblende geobarometer with application to Long Valley caldera (California) volcanic rocks. Geology, 17 (9), 837–841. https://doi.org/10.1130/0091-7613(1989)017<0837:ECOTAI>2.3.CO;2

Johannsen, A. (1931). A Descriptive Petrography of the Igneous Rocks, V.1, Chicago University Press, Chicago, 267p.

Kelly, R.K, Keleman, P.B., & Jull, M. (2003). Buoyancy of the Continental Upper Mantle, Geochemistry Geophysics Geosystems, 4(2), 1-24. Doi: 10.1029/2002GC000399

Kuehn, S.C., & Foit, F.F.Jr. (2006). Correlation of widespread Holocene and Pleistocene tephra layers from Newberry Volcano, Oregon, USA, using glass compositions and numerical analysis. Quaternary International, 148(1), 113-137. https://doi.org/10.1016/j.quaint.2005.11.008

Klein, C. (2005). Some Precambrian banded iron-formations (BIFs) from around the world: Their age, geologic setting, mineralogy, metamorphism, geochemistry, and origins. American Mineralogist, 90(10), 1473-1499. doi.org/10.2138/am.2005.1871

Kress, V.C., & Carmichael, I.S.E. (1991). The compressibility of silicate liquids containing Fe2O3 and the effect of composition, temperature, oxygen fugacity and pressure on their redox states. Contributions to Mineralogy and Petrology, 108(1-2), 82-92 doi.org/10.1007/BF00307328

Lapointe, P., Morris, W.A., & Harding, K.L. (1986). Interpretation of magnetic susceptibility: a new approach to geophysical evaluation of the degree of rock alteration. Canadian Journal of Earth Sciences, 23(3), 393-401.

Le Maitre, R.W., Streckeisen, A.B., Zanettin, A.B., Le Bas, M.J., Bonin, P. Bateman, P., Belleini, G., Dudek, A., Efremova, S., Keller, J., Lemayre, J., Sabine, P.A.., Schmid, R., Sorensen, H., & Wooley, A.R., (2005). Igneous Rocks: A Classification and Glossary of Terms: Recommendations of the International Union of Geosciences Sub-Commission on the systematics of igneous rocks. Cambridge University Press, 237p.

Lesage, G., Byrne, K., Morris, W.A., Enkin, R.J., Lee, R.G., Mir, R., & Hart, C.J.R. (2019). Interpreting regional 3D fault networks from integrated geological and geophysical data sets: An example from the Guichon Creek batholith, British Columbia. Journal of Structural Geology, 119, p.93-106.

Loucks, R.R. (1996). A precise olivine-augite Mg-Fe-exchange geothermometer. Contributions to Mineralogy and Petrology, 125(2–3), 140–150. doi.org/10.1007/s004100050211

Mahmoodi, O. & Smith, R. (2015). Clustering of downhole physical property measurements at the Victoria property, Sudbury for the purpose of extracting lithological information. Journal of Applied Geophysics, 118, 145-154.

Malinverno, A., & Pohlman, J.W. (2011). Modeling sulfate reduction in methane hydrate-bearing continental margin sediments: Does a sulfate-methane transition require anaerobic oxidation of methane? Geochemistry, Geophysics, Geosystems, 12(7), 1-18. DOI: 10.1029/2011GC003501

Malvoisin, B., Carlut, J., & Brunet, F. (2012). Serpentinization of oceanic peridotites: 1. A high-sensitivity method to monitor magnetite production in hydrothermal experiments. Journal of Geophysical Research, 117, B01104. DOI:10.1029/2011JB008612.

Marakushev, A.A. (1971). Petrochemical systematics of igneous and metamorphic rocks. International Geology Review, 17(2), 191-202, DOI.org/10.1080/00206817509471716

Mccammon, C., & Kopylova, M.G. (2004.) A redox profile of the Slave mantle and oxygen fugacity control in the cratonic mantle. Contributions to Mineralogy and Petrology, 148(1), 55-68. DOI: 10.1007/s00410-004-0583-1

McCuaig, T.C., & Hronsky, J.M.A. (2014). The mineral system concept: the key to exploration targeting. Society of Exploration Geologists, Special Publication 18, 153-175.

Middlemost, E.A.K., (1989). Iron oxidation ratios, norms and the classification of volcanic rocks. Chemical Geology, 77(1), 19-26, doi.org/10.1016/0009-2541(89)90011-9

Morris, B., Ugalde, H., & Thompson, V. (2007). Magnetic remanence constraints on magnetic inversion models. The Leading Edge, 26(8), 960-964.

Mutch, E.J.F., Blundy, J.D., Tattitch, B.C., Cooper, F.J., & Brooker, R.A., (2016). An experimental study of amphibole stability in low-pressure granitic magmas and a revised Al-in-hornblende geobarometer. Contributions to Mineralogy and Petrology, 171(85), 27p. https://doi.org/10.1007/s00410-016-1298-9

Parker Gay, S., & Hawley, B.W. (1991). Syngenetic magnetic anomaly sources: Three examples. Geophysics, 56, 902-913.

Peters, C., & Dekkers, M.J. (2003). Selected room temperature magnetic parameters as a function of mineralogy, concentration and grain size. Physics and Chemistry of the Earth, 28, 659–667.

Peters, D., Bretscher, A., John, T., Scambelluri, M., & Pettki, T. (2017). Fluid-mobile elements in serpentinites: Constraints on serpentinisation environments and element cycling in subduction zones. Chemical Geology, 466(5), 654-666. doi.org/10.1016/j.chemgeo.2017.07.017

Platt, R., & Woolley, A. (1986). The mafic mineralogy of the peralkaline syenites and granites of the Mulanje complex, Malawi. Mineralogical Magazine, 50(355), 85-99. doi:10.1180/minmag.1986.050.355.12

Pohlman, J.W., Riedel, M., Bauer, J.E., Canuel, E.A., Paull, C.K., Lapham, L., Grabowski, K.S., Coffin, R.B., Spence, G.D. (2013). Anaerobic methane oxidation in low-organic content methane seep sediments. Geochimica et Cosmochimica Acta., 108, 184-201. DOI: 10.1016/j.gca.2013.01.022

Potts, P.J. (1987). Classical and rapid methods of analysis. p.47-76., In: A Handbook of Silicate Rock Analysis, Springer, Dordrecht. doi.org/10.1007/978-94-015-3988-3_2

Pozza, M.R., Boyce, J.I., & Morris, W.A. (2004). Lake-based magnetic mapping of contaminated sediment distribution, Hamilton Harbour, Lake Ontario, Canada. Journal of Applied Geophysics, 57, 23-41.

Puga, E., Ruiz Cruz, M.D., & Diaz de Frederico, A. (1999). Magnetite – Silicate inclusions in olivine of ophiolitic metagabbros from the Mulhacen Complex, Betic Cordillera, South Eastern Spain. The Canadian Mineralogist, 37, 1191-1209.

Puranen, R. (1989). Susceptibilities, iron and magnetite content of Precambrian rocks in Finland. Geological Survey of Finland, Report of Investigation 90.

Ravna, E.K. (2000). The garnet–clinopyroxene Fe2+–Mg geothermometer: an updated calibration. Journal of Metamorphic Geol., 18, 211-219.

Robie, R.A., Finch, C.A., & Hemingway, B.S. (1982). Heat capacity and entropy of fayalite (Fe2SiO4) between 5.1 and 383 K: comparison of calorimetric and equilibrium values for the QFM buffer reaction. American Mineralogist, 67(5-6), 463–469.

Roy, B., & Clowes, R. M. (2000). Seismic and potential-field imaging of the Guichon Creek batholith, British Columbia, Canada, to delineate structures hosting porphyry copper deposits. Geophysics, 66(5), 1418-1434.

Rutter, M.J., Van der Laan, S.R., & Wyllie, P.J. (1989). Experimental data for a proposed empirical igneous geobarometer: Aluminum in hornblende at 10 kbar pressure. Geology, V.17, no.10, p.897–900. doi: https://doi.org/10.1130/0091-7613(1989)017<0897:EDFAPE>2.3.CO;2

Sawyer, E.W., Cesare, B., & Brown, M. (2011). When the Continental Crust Melts. Elements, 7(4), 229-234. doi.org/10.2113/gselements.7.4.229

Saikkonen, R.J., & Rautiainen, I.A. (1993). Determination of ferrous iron in rock and mineral samples by three volumetric methods. Bulletin Of the Geological Society of Finland, 65(1), 59-63.

Schwarz, E.J. (1974). Magnetic Fabric in Massive Sulfide Deposits. Canadian Journal of Earth Sciences,, 11, 1669-1675. doi.org/10.1139/e74-165

Schwarz, E. (1991). Magnetic expressions of intrusions including magnetic aureoles. Tectonophysics, 192, 191-200.

Shang, J., Morris, W.A., Howarth, P., Levesque, J., Staenz, K., & Neville, B. (2009). Mine tailing surface mineralogy using hyperspectral imagery. Canadian Journal of Remote Sensing, 35(1), 126-141.

Siever, R., & Woodford, N. (1979). Dissolution kinetics and the weathering of mafic minerals. Geochimica et Cosmochimica Acta, 43(5),717-724.

Sossi, P.A., Foden, J.D., & Halverson, G.P. (2012). Redox-controlled iron isotope fractionation during magmatic differentiation: an example from the Red Hill intrusion, S. Tasmania. Contributions to Mineralogy and Petrology, 164(7), 757- 772. doi.org/10.1007/s00410-012-0769-x

Streckeisen, A. (1976). To each plutonic rock its proper name. Earth-Science Reviews, 12(1), 1-33. doi.org/10.1016/0012-8252(76)90052-0

Taylor, S.R. (1964). Abundance of chemical elements in the continental crust: a new table. Geochimica et Cosmochimica Acta, 28, 1273-1285.

Toft, P.B., Arkani-Hamed, J., & Haggerty, S.E. 1990. The effects of serpentinization on density and magnetic susceptibility: a petrophysical model. Physics of the Earth and Planetary Interiors, 65(1-2), 137-157. https://doi.org/10.1016/0031-9201(90)90082-9.

Thomas, M. D. (2003). Gravity signatures of massive sulfide deposits, Bathurst mining camp, New Brunswick, Canada. 799- 819. In: Goodfellow, W.D., McCutcheon, S.R., & Peters, J.M., eds., Massive sulfide deposits of the Bathurst Mining Camp, New Brunswick, and Northern Maine. Economic Geology Monograph 11.

Tschirhart, P., Morris, W.A., Mims, J., & Ugalde, H. (2019). Applying laterally varying density corrections to ground gravity and airborne gravity gradiometry data: a case study from the Bathurst Mining Camp. Canadian Journal of Earth Sciences,, 56(5), 493-503, https://doi.org/10.1139/cjes-2018-0046

Vallée, M.A., Farquharson, C.G., Morris, W.A., King, J., Byrne, K., Lesage, G., Lee, R.G., Chouteau, M., & Enkin R.J. (2019a). Comparison of geophysical inversion programs run on aeromagnetic data collected over the Highland Valley Copper district, British Columbia, Canada. Exploration Geophysics, 50(3), 310-323. DOI: 10.1080/08123985.2019.1604068

Vallée, M.A., Morris, W.A., Perrouty, S., Lee, R.G., Wasyliuk, K., King, J.J., Ansdell, K., Mir, R., Shamsipour, P., Farquharson, C.G., Chouteau, M., Enkin, R.J., & Smith, R.S. (2019b). Geophysical inversion contributions to mineral exploration: lessons from the Footprints project. Canadian Journal of Earth Sciences,, 56, 525-543.

Walther, J.V., & Wood, B.J. (1984) Rate and mechanism in prograde metamorphism. Contributions to Mineralogy and Petrology, 88(3), 246-259. https://doi.org/10.1007/BF00380169

Williams, N., & Dipple, G. (2007). Mapping Subsurface Alteration Using Gravity and Magnetic Inversion Models. In: Proceedings of Exploration 07: Fifth Decennial International Conference on Mineral Exploration. Ed. Milkereit, B., 461-472.

Williams, N.C. (2009). Mass and magnetic properties for 3D geological and geophysical modelling of the southern Agnew–Wiluna Greenstone Belt and Leinster nickel deposits, Western Australia. Australian Journal of Earth Sciences, 561111–1142. https://doi.org/10.1080/08120090903246220

Wilson, A.D. (1955). Determination of ferrous iron in rocks and minerals. Bulletin of the Geological Survey of Great Britain, 9, 56–58.

Worm, H-U., Clark, D., & Dekkers, M.J. (1993), Magnetic susceptibility of pyrrhotite: grain size, field and frequency dependence. Geophysical Journal International, 114, 127-137.

Wyllie, P.J. (1971). The Dynamic Earth: Textbook in Geoscience, John Wiley and Sons.

Zen, E-An. (1985). An oxygen buffer for some peraluminous granites and metamorphic rocks. American Mineralogist, 70 (1-2), 65–73. doi: https://doi.org/

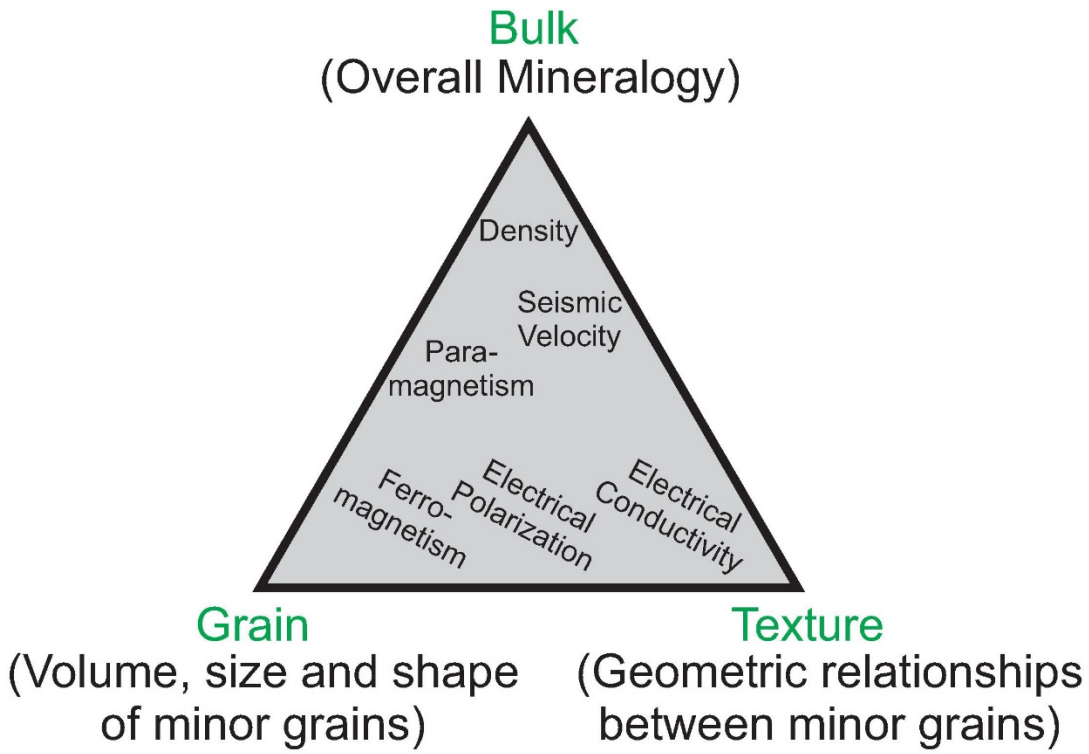

Figure 1. Triangular diagram after Dentith et al. (2017, 2019) showing how rock physical properties depend on three broad parameters expressed as bulk composition, grain properties and rock texture. Bulk composition as seen through mineralogy controls rock density by having greater or lesser proportions of dense minerals. Grain effects, particularly the concentration of ferromagnetic minerals, govern the bulk magnetic susceptibility of rocks. Rock textures such as porosity and permeability controls fluid, ion and electron pathways, which in turn controls electrical and electromagnetic phenomena such as conductivity/resistivity and chargeability. Other geophysical phenomena depend on combined effects of the three end members.

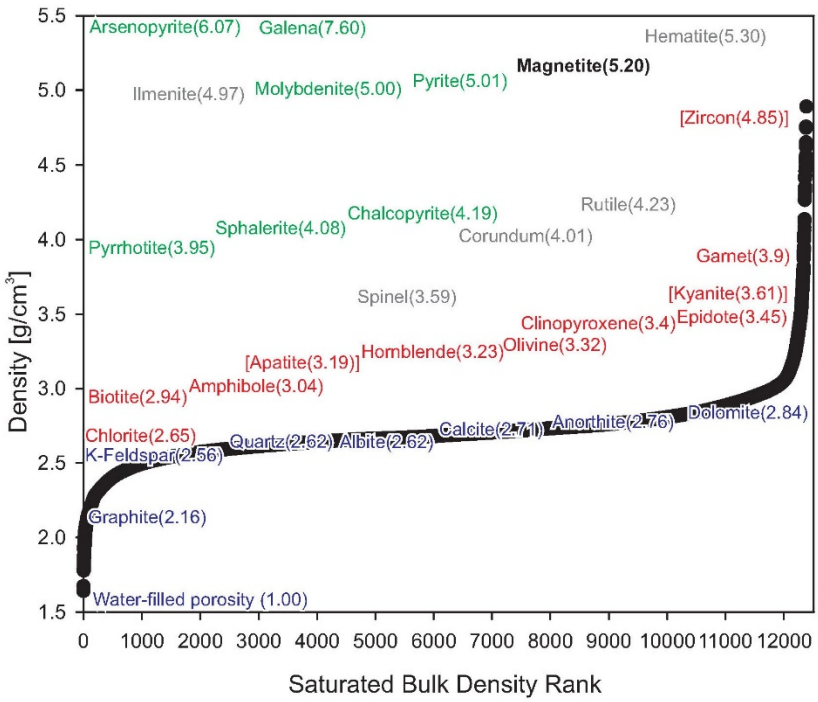

Figure 2. Plot of the ranked densities from the Canadian Rock Physical Property Database (CRPPD, Enkin, 2018) along with the mineral densities for four series of minerals: Green denotes sulfide and sulfarsenide minerals, Grey denotes oxide minerals with magnetite colored Black, Red denotes ferromagnesian silicates and other dense, non-magnetic accessory minerals, and Blue denotes the abundant rock forming silicates, carbonates, and water. Muscovite is significant in regional metamorphic rocks and has a density of about 2.82 g/cm^3 so it would fall between anorthite (calcic plagioclase) and dolomite on the figure. Most rocks contain feldspars, quartz or calcite with a few percent of one or two ferromagnesian silicates and a percent or less of oxides and sulfides and less than a few percent water content, thus have densities between 2.6 and 2.7 g/cm^3.

a)

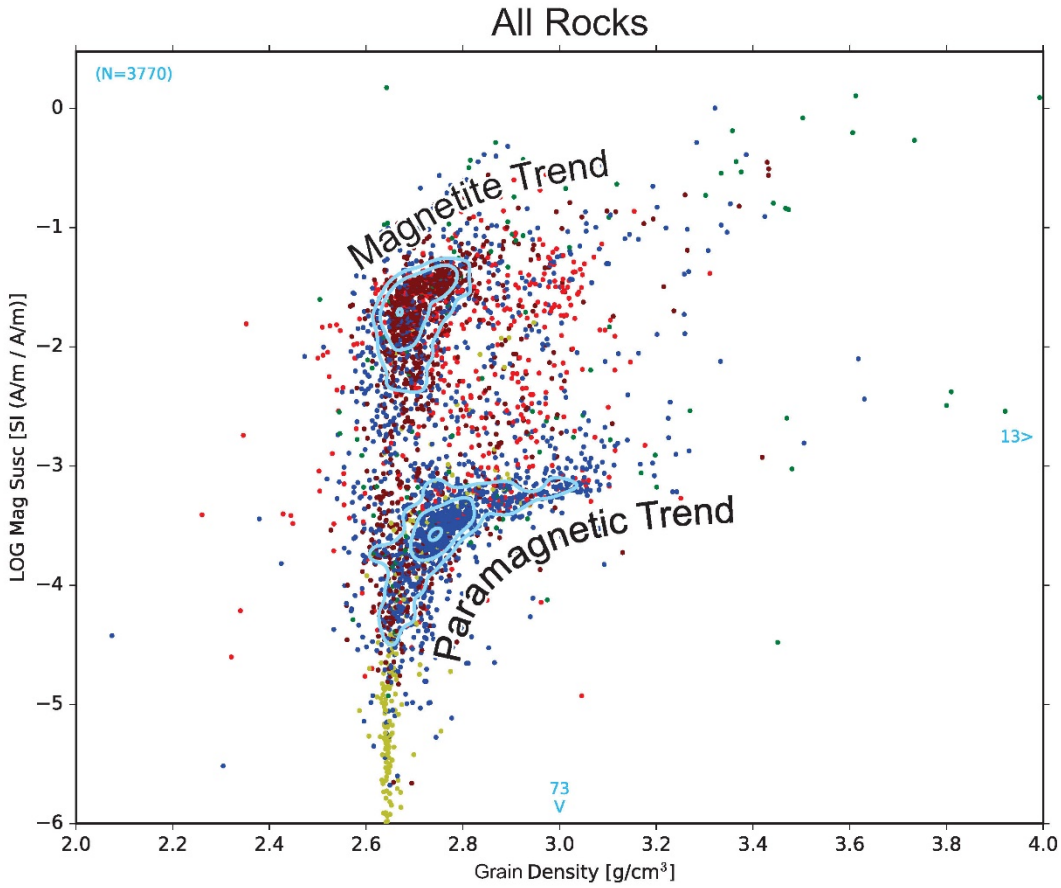
All Rocks
(N=3770)
Magnetite Trend
Paramagnetic Trend
13>
73
V
LOG Mag Susc [SI (A/m / A/m)]
Grain Density [g/cm³]

b)

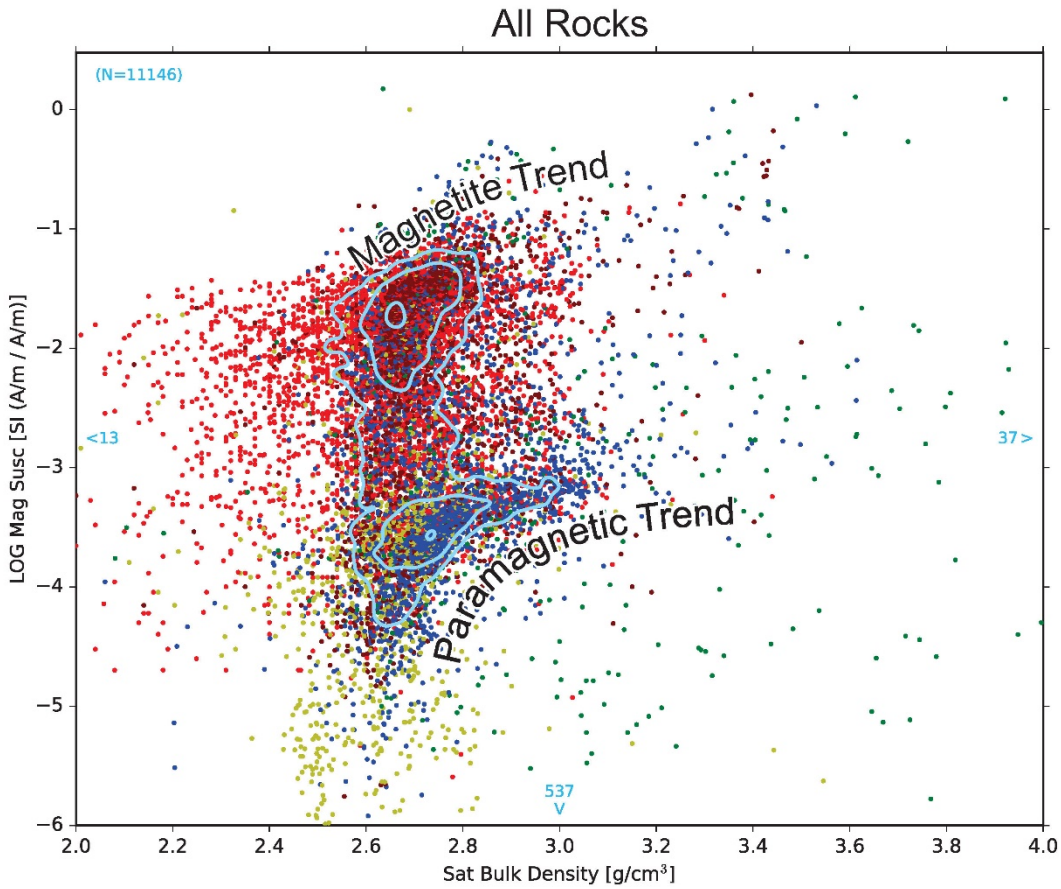
All Rocks
(N=11146)
Magnetite Trend
Paramagnetic Trend
<13
37>
537
V
LOG Mag Susc [SI (A/m / A/m)]
Sat Bulk Density [g/cm³]

Figure 3. Henkel plots (log magnetic susceptibility against density) of rock measurements compiled in the CRPPD. Lithologies: Red-volcanic, Dark Red-plutonic, Blue-metamorphic, Yellow-sedimentary and Green-mineralized or altered rocks. Many points in the database have similar values so they overlap on this plot. Point densities (after Gaussian smoothing), contoured (light blue curves) at levels of 1, 2 and 6 points per unit area, outline significant populations lying along 2 dominant trends: the magnetite trend with magnetic susceptibilities mostly above 10^{-2} SI, and the paramagnetic trend with magnetic susceptibilities below about 10^{-4} SI. **a)** The 3770 sample points with grain density (number in upper left of figure) in the CRPPD. The blue numbers on the sides mark the number of points beyond the axis on that side. **b)** The 11146 rocks with saturated bulk density measurements, which is more typically measured than grain density.

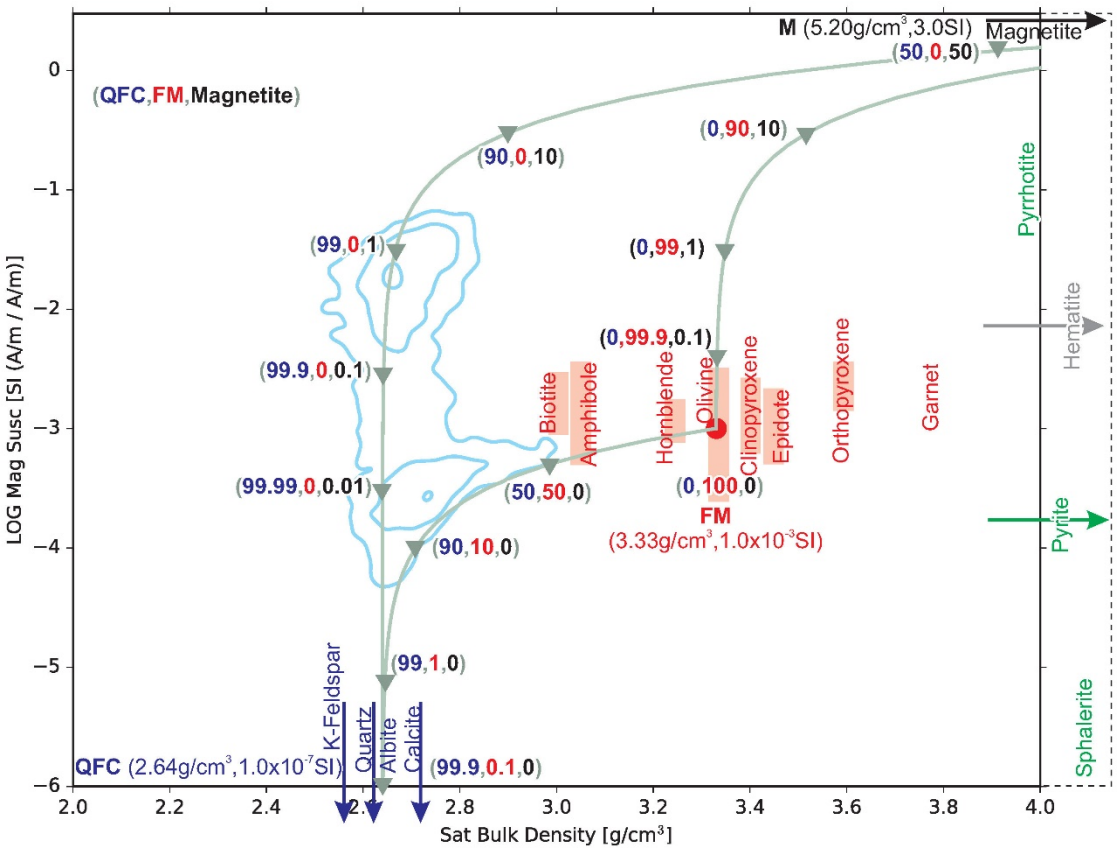

Figure 4. Calibration of the Henkel plot with volume percentages of mineral end-members chosen to span most common rock types. The blue iso-concentration contour lines from samples in the CRPPD are the same as in Figure 3b. The three mineral end members are chosen to represent how the bulk composition and the mineralogy of rocks relates to their density and magnetic susceptibility. The low density and non-magnetic components of rocks (Fig.2) typically include quartz, alkali feldspar, plagioclase, and calcite, so we choose the QFC end member (2.64 g/cm^3, 10^{-7} SI). The magnetic susceptibility of most rocks is mainly due to their magnetite content, component M (5.20 g/cm^3, 3.0 SI). Ferromagnesian silicates including biotite, hornblende, pyroxene and olivine have a wider range of density and susceptibility, and these are dependent on their iron content. The representative point (3.33 g/cm^3, 10^{-3} SI) chosen for the FM endpoint is based on the dominant density of olivine, the density of deep crust, and the shape of the CRPPD iso-concentration contours. The grey boundary lines are mixing lines due to closure. The values posted at the grey triangles are ordered triples (Blue=QFC, Red=FM, Black=Magnetite). The base of the mixing model is for "white and black" (QFC – FM) rock with zero magnetite. The left side of the plot is the mixing line between pure QFC and M. The right side marks mixing line between FM and M. Adding dense minerals moves the density to the right.

a)

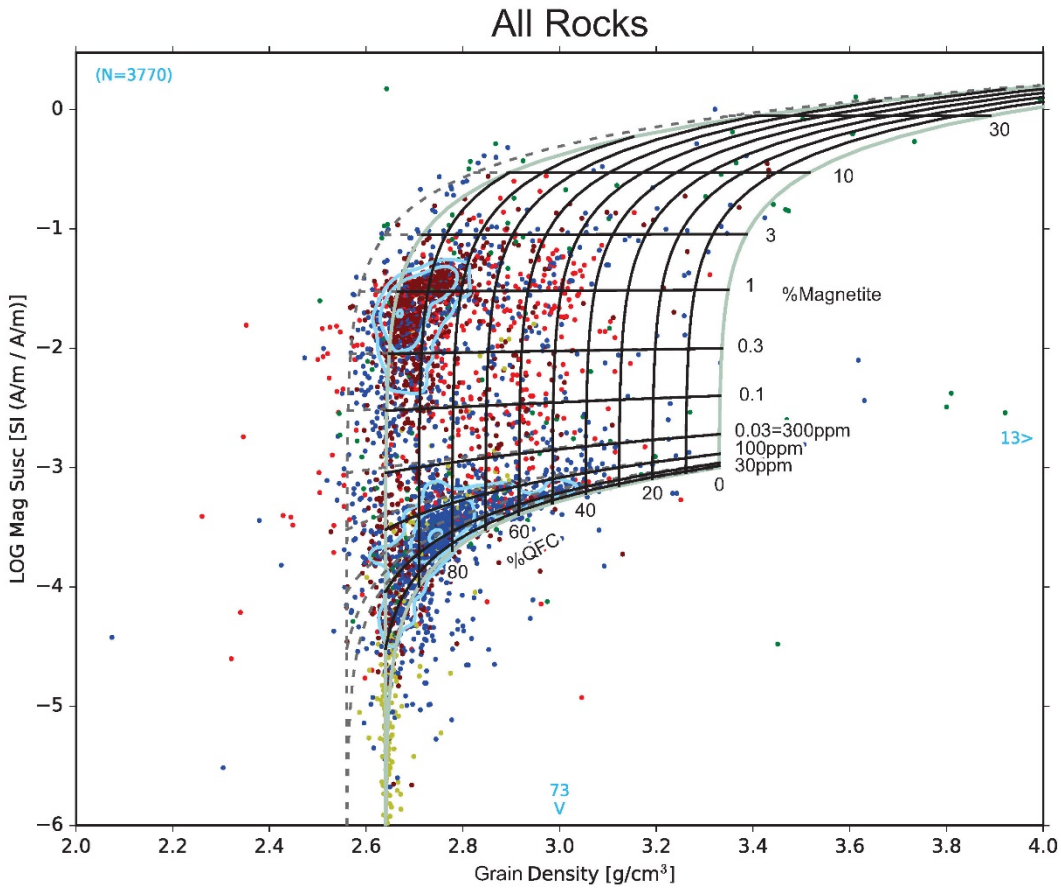
All Rocks
(N=3770)
30
10
3
1
%Magnetite
0.3
0.1
0.03=300ppm
100ppm
30ppm
0
20
40
60
%QFC
80
13>
73
V
LOG Mag Susc [SI (A/m / A/m)]
Grain Density [g/cm³]

b)

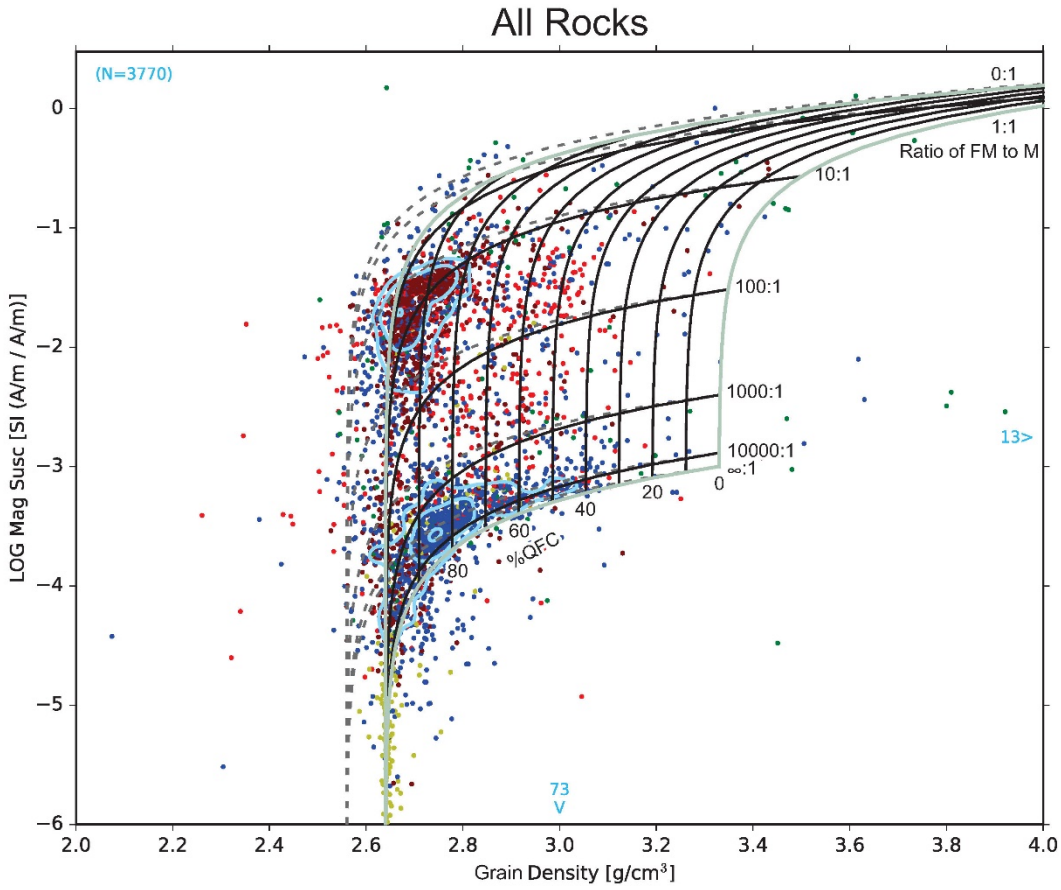
All Rocks
(N=3770)
0:1
1:1
Ratio of FM to M
10:1
100:1
1000:1
10000:1
∞:1
0
20
40
60
%QFC
80
13>
73
V
LOG Mag Susc [SI (A/m / A/m)]
Grain Density [g/cm³]

Figure 5. Three-component mineral mixing curves superimposed on the Henkel plots with grain density data from the CRPPD and their iso-concentration contours (as per Fig. 3a). In both **a)** and **b)**, subvertical lines show the range of QFC volume proportions from 0 to 100% in 10% steps, with the remainder of the rock being the sum of FM and M. In **a)** logarithmic steps of magnetite content, M (volume proportions), are drawn as percentages for the subhorizontal lines. For magnetite content M>0.03% these lines are essentially horizontal, meaning that magnetic susceptibility is directly proportional to magnetite content. Most igneous rocks have 0.2%<M<2% and QFC>70%, essentially granodiorites, granites and felsic volcanics. For rocks containing substantial amounts of lower-density K-feldspar (2.56 g/cm^3), the dashed lines show the shift to the QFC-MF-M mixing curves. In **b)**, logarithmic steps of the volume ratio of the FM mineral component to Magnetite magnetite content are drawn. The magnetite trend is centered along the FM/M value of 10. Rocks along the paramagnetic trend have lost most of their ferric iron so that they commonly have FM/M volume ratios > 1000.

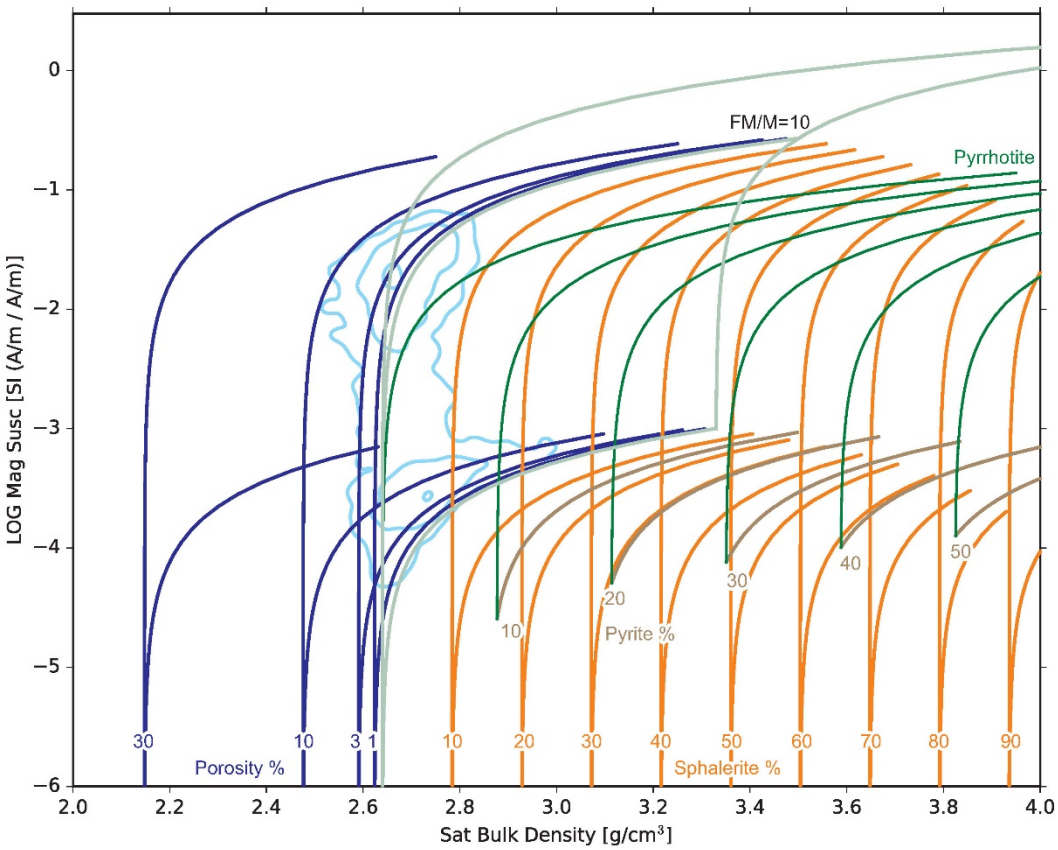

Figure 6. The Henkel plot showing projections out of the QFC-FM-M plane due to the effects of water and sulfide mineral components. The CRPPD iso-concentration contours and bounding grey mineral mixing curves of Figures 4 display where most rock measurements plot. The curves for the paramagnetic trend (~M=0) and the magnetite trend (FM/M = 10) are replotted with varying proportions of water (density 1.0 g/cm^3, blue) revealing the reduction in saturated bulk density with increasing porosity, and a non-magnetic sulfide (the pure Zn end member of sphalerite, 4.08 g/cm^3, in orange) which makes the density increase. The QFC+MF mixing curves with varying proportions of the most common sulfide mineral, pyrite (5.01 g/cm^3, $2.5 \cdot 10^{-4}$ SI) are plotted in brown. The green curves display mineral mixing models of QFC and pyrrhotite (3.95 g/cm^3, $1.4 \cdot 10^{-1}$ SI) with varying proportions of pyrite.

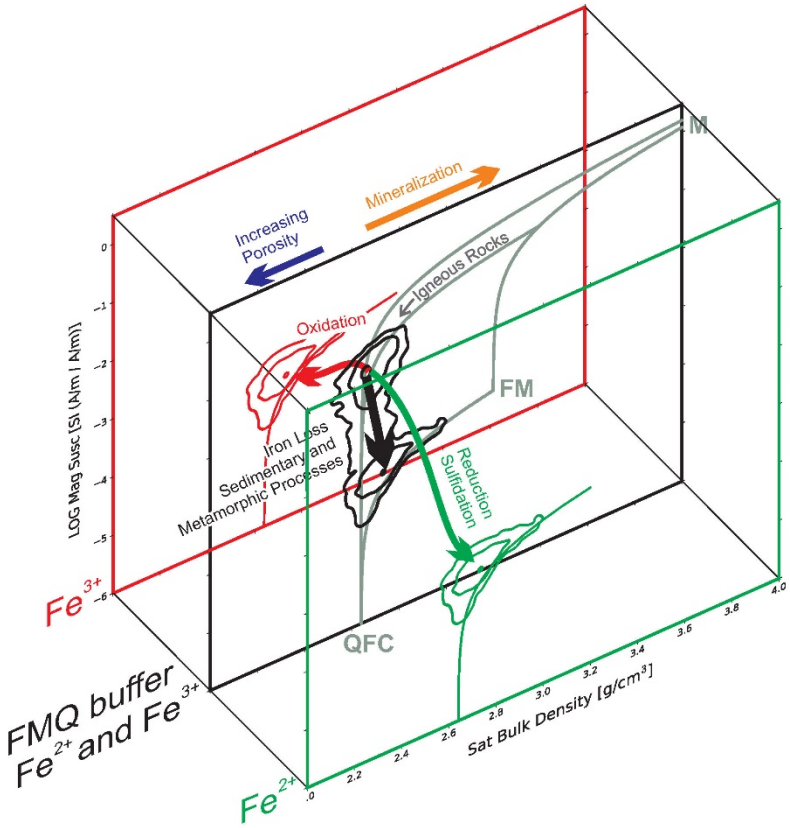

Figure 7. Expanded 3-D Henkel plot to include: oxidation, reduction and other geological processes. Figures 3 through 6 all treat the Henkel plot as a plane. That plane, including the maximum magnetite proportion set by the FMQ oxygen buffer, is shown in black in the middle of this diagram with the grey boundaries and QFC, FM and M end members as per figures 4. The dominant magnetite content for igneous rocks, as indicated by the upper bulls eye in black for the distribution of rocks in the CRPPD. The back plane in red denotes complete oxidation to ferric hematite or oxyhydroxides, and the oxidizing trend, following the red arrow, shown in projection, points to diminished magnetic susceptibility by one or more orders of magnitude. The front plane in green denotes complete reduction to 100% ferrous iron and the loss of magnetite or any other ferric minerals. The green arrow indicating reduction typically occurs by sulfidation and ore genesis in igneous and metamorphic rocks. In anoxic sedimentary rocks, the reduction is a biogeochemical process due to organic carbon content and burial diagenesis, or sulfidation by the reduction of sulfate anions, in the absence of free oxygen. With sulfidation and reduction of ferric to ferrous iron, as shown by the green arrow, density will be moved down and to higher density (orange arrow). The black arrow in the ordinary plane denotes iron loss in sedimentary processes such as mechanical weathering and dissolution in during transport and exposure to water, or prograde metamorphism via dissolution and fluid losses. The blue arrow denotes the addition of porosity and low density water.

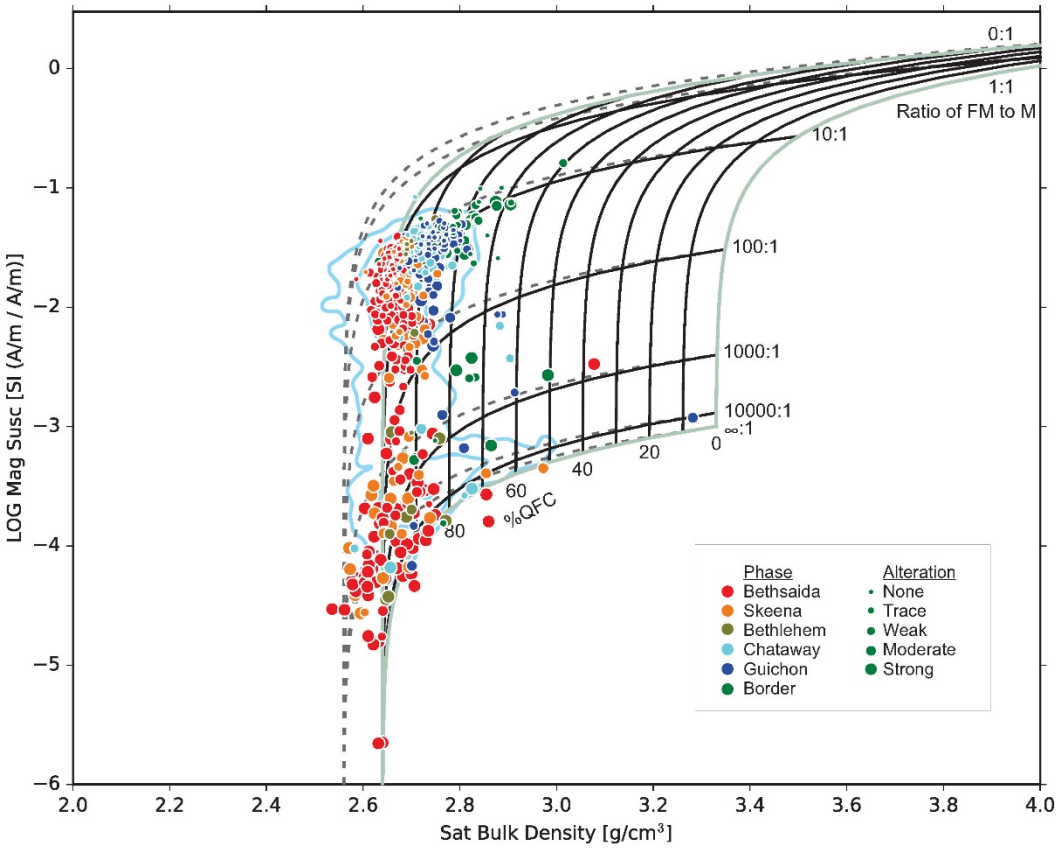

Figure 8. Example revealing the effects of primary mineralogy, alteration and mineralization as seen on the Henkel plot. The samples are from the Guichon Batholith (Byrne et al., 2019, Lessage, et al., 2019), including the Highland Valley Cu-Au porphyry deposit, plotted on the Henkel plot, with blue iso-concentration contours from the CRPPD and the mineral mixing model as per Figure 5b. In the legend block, "Phase" denotes different intrusions within this nested calc-alkaline batholith. The outer, oldest and most mafic is on the bottom (Border) and central, youngest and most felsic is on the top (Bethsaida). The smallest dots are the least altered rocks retaining primary igneous mineralogy, while progressively larger dots denote more alteration and secondary mineralization. The least altered rocks follow the magnetite trend with FM/M about 10. The alteration and economic mineralization is magnetite destructive and falls at or below FM/M ~1000. In this porphyry copper deposit, alteration (and sulfide mineralization) is destructive of magnetite. The K-feldspar rich granites from the Bethseida and Skeena phases plot to the left of the grey QFC-M boundary because of they contain large proportions of K-feldspar, modelled with the dashed lines.

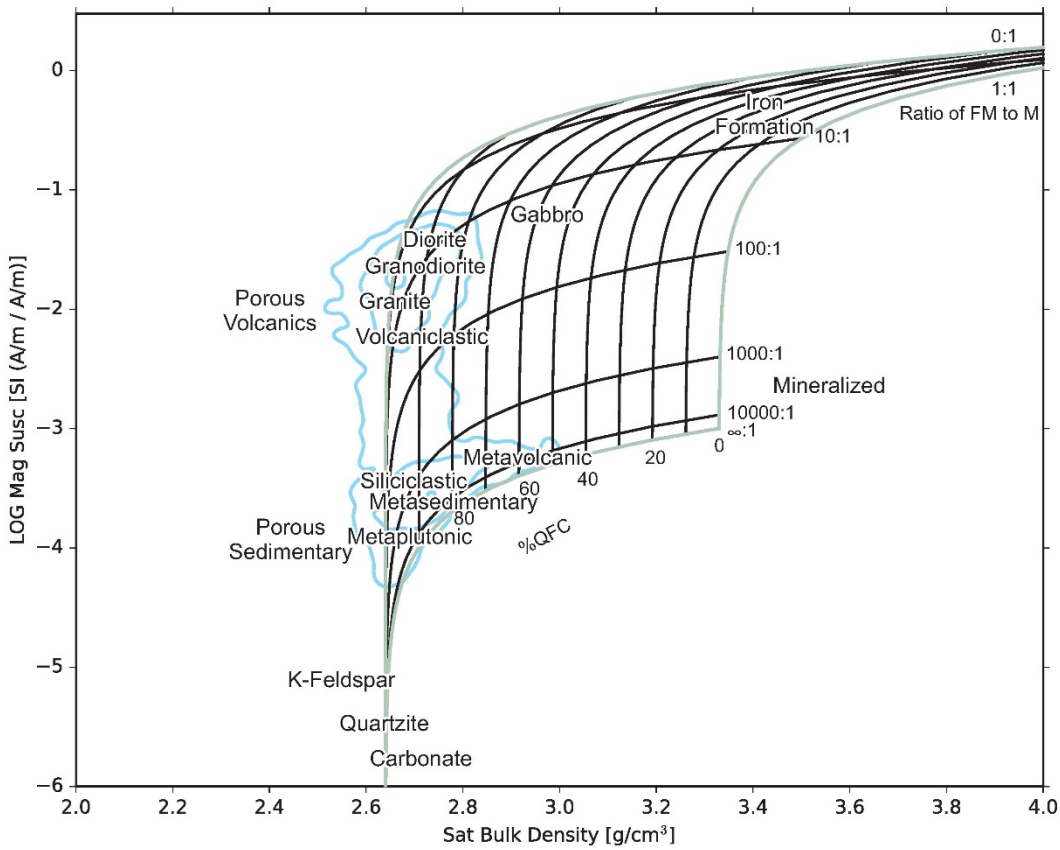

Figure 9. General locations of rock types on the Henkel plot, with blue iso-concentration contours from the CRPPD and the mineral mixing model as per Figure 5b. The source diagrams for each rock type are given in Enkin (2018) figures 16-19. Igneous rocks tend to fall along the FM/M=10 line, while metamorphic and sedimentary rocks fall on FM/N>1000. Porous rocks have lower densities while mineralized rocks have higher densities. See text for details of the locations of the different rock types. Geophysical models, which require substantial volumes of rocks with lithologies or physical properties outside the model bounds are not reasonable.